



RESEARCH ARTICLE

WILEY

Estimating water fluxes in the critical zone using water stable isotope approaches in the Groundnut and Ferlo basins of Senegal

Djim M. L. Diongue¹  | Christine Stumpp²  | Olivier Rousard^{3,4,5} |
Didier Orange^{3,6} | Frederic C. Do^{3,6} | Serigne Faye¹

¹Geology Department, Cheikh Anta Diop University of Dakar, Dakar, Senegal

²University of Natural Resources and Life Sciences, Vienna, Department of Water, Atmosphere and Environment, Institute of Soil Physics and Rural Water Management, Vienna, Austria

³LMI IESOL, IRD, ISRA, Bel Air, Dakar, Senegal

⁴CIRAD, UMR Eco&Sols, BP1386, CP18524, Dakar, Senegal

⁵Eco&Sols, Univ Montpellier, CIRAD, INRAE, IRD, Institut Agro, Montpellier, France

⁶IRD, UMR Eco & Sols, U. Montpellier, IRD, CIRAD, INRAE, Montpellier, France

Correspondence

Djim M. L. Diongue, Geology Department, Diop University of Dakar, Dakar, Senegal.
Email: djimouhamadou.diongue@ucad.edu.sn

Funding information

Agropolis Fondation; ANR-11-LABX-0010; Centre de Coopération Internationale en Recherche Agronomique pour le Développement; CGIAR; EDEQUE/UCAD; EU-DESIRA; EU-H2020; EU-LEAP-Agri; Institut de Recherche pour le Développement; TOTAL Foundations

Abstract

Sustainable water management in semi-arid agriculture practices requires quantitative knowledge of water fluxes within the soil-vegetation-atmosphere system. Therefore, we used stable-isotope approaches to evaluate evaporation (E_a), transpiration (T_a), and groundwater recharge (R) at sites in Senegal's Groundnut basin and Ferlo Valley pasture region during the pre-monsoon, monsoon, and post-monsoon seasons of 2021. The approaches were based upon (i) the isothermal evaporation model (for quantifying E_a); (ii) water and isotope mass balances (to partition E_a and T_a for groundnut and pasture); and (iii) the piston displacement method (for estimating R). E_a losses derived from the isothermal evaporation model corresponded primarily to Stage II evaporation, and ranged from 0.02 to 0.09 mm d⁻¹ in the Groundnut basin, versus 0.02–0.11 mm d⁻¹ in Ferlo. At the groundnut site, E_a rates ranged from 0.01 to 0.69 mm d⁻¹; T_a was in the range 0.55–2.29 mm d⁻¹; and the T_a/E_a ratio was 74%–90%. At the pasture site, the ranges were 0.02–0.39 mm d⁻¹ for E_a ; 0.9–1.69 mm d⁻¹ for T_a ; and 62–90% for T_a/E_a . The ET_a value derived for the groundnut site via the isotope approach was similar to those from eddy covariance measurements, and also to the results from the previous validated HYDRUS-1D model. However, the HYDRUS-1D model gave a lower T_a/E_a ratio (23.2%). The computed groundwater recharge for the groundnut site amounted to less than 2% of the local annual precipitation. Recommendations are made regarding protocols for preventing changes to isotopic compositions of water in samples that are collected in remote arid regions, but must be analysed days later. The article ends with suggestions for studies to follow up on evidence that local aquifers are being recharged via preferential pathways.

KEYWORDS

evapotranspiration, recharge, semi-arid, stable isotopes, water balance

1 | INTRODUCTION

The vadose zone—the variably saturated zone between the surface of the ground and the permanent water table (Stumpp & Kammerer, 2022)—is important to the hydrological cycle because it is the portion of the

subsurface from which precipitation either returns to the atmosphere via evapotranspiration (ET_a), or else is distributed via runoff, infiltration, and deep drainage. The latter processes contribute to food and water security by providing water to plants and contributing to groundwater recharge—a vital phenomenon in semi-arid regions, where groundwater is the single,

most reliable, and most resilient source of water for drinking, industry, and irrigation. Identification of groundwater-recharge (R) mechanisms in semi-arid regions is especially difficult due to the mechanisms' high spatial and temporal variability (Koeniger et al., 2016; Scanlon et al., 2006). Quantification of atmospheric losses (ET_a) in these regions—particularly the relative contributions of soil evaporation (E_a) and plant transpiration (T_a)—is additional challenge (Sprenger et al., 2017). As a result, important gaps exist in the research community's understanding of arid regions' hydrological processes, and of the associated water-flux partitionings within the soil-vegetation-atmosphere (SVA). Filling those gaps is crucial because semi-arid regions are highly sensitive to the projected changes in climate (Pörtner et al., 2022).

Water-flux partitioning within the SVA can be estimated either by modelling, or experimentally. The modelling approaches are commonly categorized as either analytical methods for estimating ET_a partitioning (e.g., Shuttleworth and Wallace, (1985); FAO dual Kc (Allen et al., 1998)), or numerical models, which can also estimate R (e.g., HYDRUS-1D (Šimůnek et al., 2008); SWAP (van Dam et al., 2008); SISPAT (Braud, 2002)). The experimental approaches include hydrometric methods such as the eddy covariance technique for estimating ET_a (e.g., Baldocchi, 2014; Rouspard et al., 2006; Zahn et al., 2022), and sap-flow measurements for estimating T_a (e.g., Chen et al., 2022; Do et al., 2008; Granier, 1985). Other experimental approaches for estimating ET_a or E_a are soil flux chambers (e.g., Lu et al., 2017; Raz-Yaseef et al., 2010) and (micro-) lysimeter measurements (e.g., Gong et al., 2020; Kelliher et al., 1992; Liu et al., 2022). These experimental approaches require sophisticated, expensive, high-maintenance instruments. Another experimental, data-driven method is based upon analyses of stable isotopes of hydrogen (δ^2H) and oxygen ($\delta^{18}O$) in the various water fluxes. This method can provide time-integrative information on these fluxes even in remote areas (Adomako et al., 2010; Mueller et al., 2014).

In semi-arid regions, water stable isotopes have been used successfully as environmental tracers for studying fluxes such as infiltration (e.g., Allison & Hughes, 1983; Dincer et al., 1974) and groundwater recharge (e.g., Boumaiza et al., 2021; Faye et al., 2019; Gaj et al., 2016; Koeniger et al., 2016; Scanlon et al., 2006). These isotopes have also been used to investigate evapotranspiration (e.g., Barnes & Allison, 1988; Dubbert et al., 2013; Skrzypek et al., 2015; Wang et al., 2012); uptake of water by plant roots (e.g., Dawson & Ehleringer, 1991; Xu et al., 2021; Yang et al., 2010); and hydraulic redistribution (e.g., Caldwell et al., 1998; Dawson, 1993; Oerter et al., 2021; Priyadarshini et al., 2016). Some authors have used water stable isotopes to study flow pathways and mixing in the unsaturated zone (e.g., Mueller et al., 2014; Stumpp & Maloszewski, 2010; Windhorst et al., 2014).

The evaporation fronts within the unsaturated zone have been a particular target of previous works that used water stable isotopes (Allison & Barnes, 1983; Dawson & Ehleringer, 1998). One such study (Zimmermann et al., 1967) showed that at the surface of a saturated soil column, evaporation enriches the soil water in heavy isotopes. The enrichment then decreases exponentially with depth. Formation of the similar enrichment profiles was confirmed by follow-up studies, which developed theories (e.g., isothermal evaporation) to explain

them (Allison & Barnes, 1983, 1985; Barnes & Allison, 1988; Christmann & Sonntag, 1987). For example, Allison and Barnes (1983) have shown that in a soil that has been subject to evaporation, the observed isotope profiles result from a balance between the upward evaporative flux and the downward diffusive flux. According to Allison and Barnes (1983), the assumption that the evaporative loss occurs isothermally and at thermodynamic equilibrium is reasonable as long as sufficient time has elapsed since the preceding rainfall event, so that the soil's hydrological parameters are not changing rapidly. This condition is generally satisfied in arid regions, except during the period immediately after a rainfall event (Barnes & Allison, 1988).

Quantitative calculations of groundwater recharge (R) have been another target of studies that employed water stable isotopes as tracers (e.g., Allison et al., 1983; Beyer et al., 2015). These studies have been addressed actively in older and recent reviews (Allison et al., 1994; Koeniger et al., 2016; Scanlon et al., 2002). In one study, Allison et al. (1983) developed the piston displacement method, which has proven to be a simple and suitable technique for making quantitative estimates of groundwater recharge in semi-arid climates (e.g., Boumaiza et al., 2021; Gaj et al., 2016). However, we note that the relationship on which this technique is based is empirical (Barnes & Allison, 1988), and may be site-specific. The few subsequent investigations of this relationship (e.g., Herczeg & Leaney, 2011; Selaolo et al., 2003) did not confirm it. Therefore, its applicability may be limited.

The use of stable isotopes to study ET_a partitioning (into T_a and E_a) has benefitted recently from the advent of new laser spectrometers that can analyse even small amounts of water—such as samples extracted from soils. In addition, stable isotopes in soil pore water can be analysed using the water-vapour-equilibrium method (Wassenaar et al., 2008). For example, Wenninger et al. (2010) and Sutanto et al. (2012) used a combination of lysimeter measurements and stable-isotope analyses to calculate the partitioning of ET_a for grass vegetation in laboratory setups. The necessary calculations were based upon mass balances of water and isotopes in the soils of those setups. Subsequently, Liebhard et al. (2022) successfully adapted these laboratory experiments to soybean crops under field conditions, based upon the assumption that the isotopic composition of the transpired (δ_{T_a}) water fraction is related to a crop-specific root-water uptake profile. The authors combined hourly weather data with measured ET_a rates to calculate the fractionation factors for each evaluation period. In addition, the authors based their determinations of δ_{E_a} upon isotope ratios in the evaporation zone near the soil surface, rather than in the mean soil column. However, the methods that Liebhard et al. (2022) used in soybean fields may be less suitable for arid regions, where lysimeters are difficult to instal and maintain. Other concerns include the possibility of a flow-edge effect (due to the drying of the soil) and sensitivity to different vegetation conditions inside and outside of the lysimeter (Nouri et al., 2013).

In summary, although researchers have made significant progress in using stable-isotopes approaches for estimating water-flux components in (semi-) arid regions (e.g., Adomako et al., 2010; Beyer et al., 2015; Gaj et al., 2016; Gaye & Edmunds, 1996; Koeniger et al., 2016; Rothfuss et al., 2021; Sutanto et al., 2012), few researchers have studied ET_a partitioning, particularly in rainfed

agriculture practices of (semi-) arid regions. Therefore, we used stable-isotopes approaches to investigate hydrological fluxes in Senegal's principal rainfed-agriculture region (the Groundnut basin, comprising 70% of Senegal's arable land (Faye & Du, 2021)) and in Senegal's dryer Ferlo region, where livestock grazing is the main agricultural activity. Information on ET_a partitioning and quantitative R estimation in the two regions is very limited, despite the region's importance to Senegal's water and food security. As one example of that importance, statistics from Senegal's National Agency for Statistics and Demography (ANSD) show that in 2020, 63.15% of the nation's total planting area was devoted to raising groundnut (also known as peanut, *Arachis hypogaea* L). The Ferlo region's importance is similar. There, extensive livestock-raising is the most important source of food and income for many households, including the region's semi-transhumant and semi-nomadic pastoralists (Niemi et al., 2015).

The specific objectives of our study are to use different isotope approaches to (1) quantify E_a ; (2) partition E_a and T_a for groundnut crops and natural pasture vegetation; (3) estimate R; and (4) compare these results to those from numerical-modelling approaches that have been carried out in the Groundnut basin experimental site (Diongue et al., 2022). We formulate three hypotheses: (i) that E_a can be estimated

accurately from soil-water isotope profiles (because the necessary isothermal equilibrium is maintained); (ii) that the isotopic composition of the transpired water (δ_{T_a}) fraction is related to a specific root-water uptake profile (and therefore that both E_a and T_a can be partitioned by calculating mass balances for water and isotopes); and (iii) that the assumption of piston flow is valid for the studied environment, and can therefore be used to estimate groundwater-recharge rates (R).

2 | MATERIALS AND METHODS

The research described in this section was performed during 2019–2021.

2.1 | Study sites

The two sites selected for this study are located in mid-western and northern Senegal, along a rainfall gradient decreasing from south to north (Figure 1). Site 1 is located in the agro-ecological zone of Groundnut basin (mid-western part of Senegal) in the region of Fatick

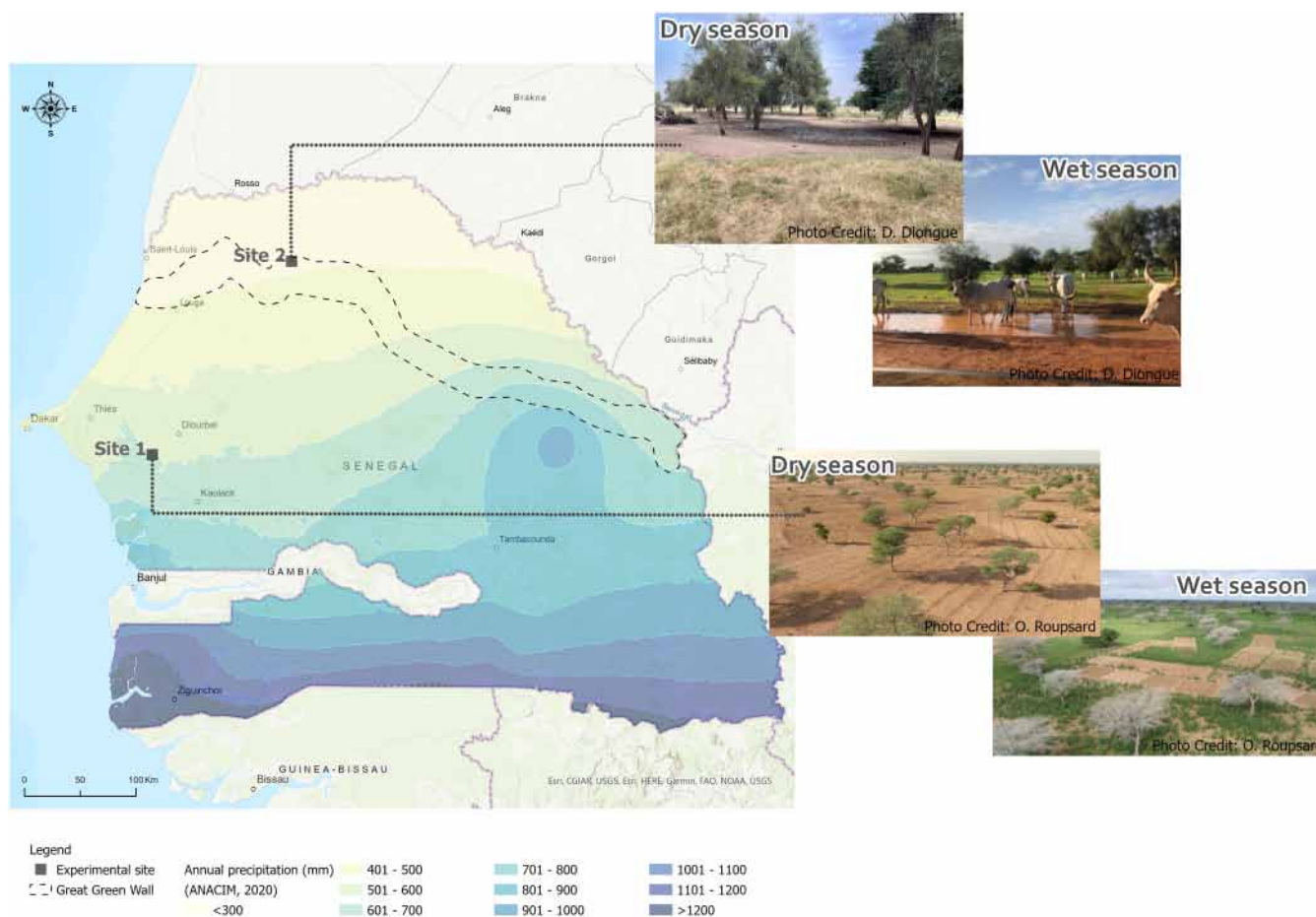


FIGURE 1 Locations of the two study areas. Site 1 is in the groundnut basin, within an agroforestry park dominated by *Faidherbia albida* trees that are associated with rainfed groundnut crops. Site 2 is located in the Ferlo Valley within the Great Green Wall, near a temporary pond used by Peul herders to water their cattle during the rainy season. Vegetation at site 2 is dominated by thorny species such as *Balanites aegyptiaca*, and is influenced by seasonal grazing. The annual-precipitation basemap is from Agence nationale de l'Aviation Civile et de la Météorologie (ANACIM). Photos show the sites' landscapes during the dry and rainy seasons.

(135 km from Dakar), where rainfed agriculture is the dominant activity. Site 2 is located in the silvo-pastoral zone of the Ferlo Valley (northern part of Senegal) in the region of Louga (400 km from Dakar), where livestock farming is the main activity.

2.1.1 | Site 1: Groundnut basin

Site 1 is part of the “Faidherbia-Flux” (FLUXNET/SN-Nkr) collaborative platform (<https://lped.info/wikiObsSN/?Faidherbia-Flux>) in the agroforestry parkland of Sob village. The landscape is flat with a gentle northward slope, characterized by a tree-based cropping system dominated by *Faidherbia albida* (Del.) A. Chev. The density of the stand is 6.8 trees ha⁻¹, and the canopy cover is 9.6% (Roupsard et al., 2020). *Faidherbia* is a nitrogen-fixing species with a reverse phenology (i.e., it has no leaves during rainy season). It is known to boost the yields of associated crops (Roupsard et al., 2020; Sileshi, 2016). During the rainy season, farmers in the agroforestry zone raise rainfed pearl millet and groundnut crops, in annual rotation. Groundnut farming accounts for over 35% of the local household revenue, and constitutes an important component of Senegal's local staple foods (Diagne, 2014).

The climate at Site 1 is of the semi-arid Soudano-Saharan type, with high temperatures (mean: 29.8°C), a high reference evapotranspiration ($ET_0 = 1500\text{--}2000\text{ mm y}^{-1}$), and a long-term mean annual rainfall of 600 mm (Faye, Diallo, et al., 2020; Faye, Fall, et al., 2020). Rainfall occurs only during the five-month rainy season (June–October). From July to September, mean monthly rainfall exceeds the ET_0 , thus allowing percolation and groundwater recharge to occur. In contrast, the dry season's high ET_0 drives evaporation from surface and soil water, and consequently may induce upward water fluxes from groundwater into the soil. During the year 2021, measured values of rainfall, ET_0 , and actual evapotranspiration (ET_a , from eddy covariance) were 478 mm, 1512 mm, and 453 mm, respectively (Diongue et al., 2022).

The soil at Site 1 is of a type known locally as “Dior soil,” and contains less than 20% clay. According to the FAO classification, it is an Arenosol (loamy sand or coarser texture). The Continental Terminal (CT) formations constitute the upper, unconfined aquifer. A shallow, brackish groundwater table is at a depth of around 6 m. The CT consists of detrital sea-origin formations that were deposited during the Cenozoic period (Oligo-Miocene to Pliocene). Later, the deposits underwent an intense ferrallitic alteration that caused crusting, significant silica movement, formation of ferruginous concretions, and neo-formation of kaolinite (Conrad & Lappartient, 1987).

2.1.2 | Site 2: Ferlo

Site 2 is located in Widou Thiengoly village near a small temporary pond (Faye et al., 2022). The area is part of the Great Green Wall zone, which was reforested with *Acacia senegalensis* (L.) and *Balanites aegyptiaca* (L.) Del. This region is characterized by intense livestock

breeding of zebu, sheep, goats, and camels. Human and livestock populations increased by a factor of about 2.3 between 1950 and 1983 (Vincke et al., 2010).

The climate is of Sahelian type (arid), with a 9-month dry season (from June to October) and a short rainy season (July to September). The annual mean temperature is 28 °C, and the mean long-term (50 years) rainfall is 371 mm (Ndiaye et al., 2015). During June to December of 2021, rainfall and ET_0 values were, respectively, 280 and 1080 mm.

The topography is mainly flat, with low, gently undulating dunes of aeolian sand that remain from erg deposits during the Middle to Recent Quaternary period (Tappan et al., 2004). The soils have loamy-sand to sandy clay-loam textures (Faye, Diallo, et al., 2020). According to the French classification, they are degraded red-brown sub-arid soils. (Or “Cambic-Luvic Arenosols” according to the FAO (Maignien, 1965)). Clay contents are less than 25%. Edaphic conditions prevailing near temporary ponds and on the slopes of dunes play a significant role in microclimate aridity, which in turn influences the soil water balance, and therefore vegetation development (Vincke et al., 2010). Vegetation consists of thorny trees, shrubs, and a seasonal herbaceous-species cover. The shrub stratum is composed mainly of *Calotropis procera* (Ait.) and *Boscia senegalensis* (L.) (Ndiaye et al., 2015; Niang, 2009). The dominant herbaceous (pasture) species during rainy seasons are *Heteropogon contortus* (L.) P.Beauv (which is investigated in the present study) and *Indigofera senegalensis* (L.) (Grouzis et al., 1998).

The temporary ponds that form during the rainy season are used for livestock needs. In addition, two aquifers provide groundwater resources: the CT aquifer (water table depth 50–70 m) and the deep Maastrichtian aquifer (200–350 m). They supply drinking water for people and livestock.

2.2 | Soil and water sampling

The sampling scheme used in this study was designed to provide the data that are needed for calculating values of E_a and T_a per the mass balances that the previous authors had applied to grass vegetation and soybean fields (Wenninger et al. (2010); Sutanto et al. (2012); and Liebhard et al. (2022)).

At both sites, daily precipitation events were sampled with a rain-fall collector (Rain Sampler RX1, Palmel Ltd, Croatia) during the 2019–2021 rainy seasons. The collector was located in an open area, at a height of 2 m. Precipitation samples were preserved in airtight vials, with an additional covering of parafilm, then stored in a refrigerator at 4 °C until they were subjected to isotope analysis. Eighty-three (83) samples were collected from Site 1, and 44 from Site 2.

Soil profiles were sampled in 2021, along gentle slope transects. Specifically, the samples were taken during February and June (bare soil, during the dry season); in December (after harvest, during the dry season); and during the August wet season, which corresponds to the growing stage of groundnut crops and pasture. At Site 1, samples were collected from the upper, middle, and lower slopes. Only the

middle and lower slopes were sampled at Site 2. Continuous soil cores were collected with a hand auger (Eijkelkamp, Netherlands). At Site 1, two core soil profiles were carried out at each slope location, from a depth of 5 cm down to the capillary fringe (500 cm below ground level at the upper and middle slopes, and 400 cm below ground level at the lower slope). One of the profiles was sampled underneath the *Faidherbia*'s canopy; the other was from an open area. At Site 2, one soil profile was collected at each slope location, in an open area, from a depth of 5 cm down to 300 cm.

During the first sampling campaign (in February), soil samples were collected at the follow depth intervals: every 5 cm, from the depth of 5 cm down to 20 cm (the critical zone), every 10 cm between 20 and 50 cm; every 25 cm between 50 and 200 cm; every 50 cm between 200 and 300 cm; and every 100 cm between 300 and 500 cm. The other sampling campaigns (in June, August, and December) used the same 5-cm interval for the topsoil (i.e., depths down to 20 cm), but larger intervals for the deeper soil zones. Immediately after each sample was collected, a 200-g sub-sample of it was stored in a labelled Ziploc® brand Double Guard freezer bag with Double Zipper Seal (ca. 1 L volume) (S. C. Johnson & Sons Inc., USA). Each sub-sample was doubled-bagged to prevent evaporative moisture loss during fieldwork. The sub-samples were then stored at 4 °C in a refrigerator for up to 3–6 days before being shipped by air to the laboratory of the Institute of Soil Physics and Rural Water Management in Vienna (Austria) for analysis. In all, 313 samples were sent from Site 1, and 68 from Site 2.

Groundwater was sampled at Site 1 in three piezometers during the 2020 wet season, and during each soil sampling campaign during 2021. Piezometers were purged for 10–15 minutes before taking samples, which were then stored in airtight vials covered with parafilm and stored at 4 °C in a refrigerator.

2.3 | Laboratory analyses

2.3.1 | Soil physical properties

To determine their textures and dry bulk densities (ρ_b), soil profiles from Site 1 were sampled with a calibrated cylinder (100 cm³). The ρ_b values were then determined in Dakar by the “Laboratoire d'Ecologie Microbienne des Sols et Agrosystèmes Tropicaux”, LMI IESOL, by weighing the soil samples after oven-drying for 48 h at 105 °C. Porosities (p) of soil samples were calculated following Black et al. (1965), assuming a particle density of 2.65 g cm⁻³.

The particle size distributions (PSDs) of samples were determined via the laser diffraction method at the laboratory of “LEHNA-ENTPE,” in Lyon, France. With these PSD results as inputs, the GRADISAT V9.1 package (Blott, 2001) was used to compute the fractions of sand, silt, and clay, and thus to classify the soil textures according to the USDA. For Site 2, we used soil-texture data from Faye, Diallo, et al. (2020), Faye, Fall, et al. (2020), which covered the 0–100 cm depth on the mid-slope locations as well as on the lower-slope locations, near the pond.

The gravimetric water content (GWC) of each soil sample (all had been stored in double Ziplock bags; Section 2.2) was determined by weighing and drying before and after isotope analyses. The volumetric water content (VWC) was calculated according to Gardner (1965), using the measured ρ_b and assuming a water density (ρ_w) of 1 g cm⁻³.

ET_a values for the groundnut crop at Site 1 were derived from latent heat (λE) flux analysis via the eddy-covariance technique. For that purpose, an antenna equipped for eddy-covariance measurements (Li-7500A (LiCor) + Windmaster Pro (Gill)) had been installed in Site 1, at a height of 4.5 m. Raw data were acquired at 20 Hz, using Tourbillon (INRAE) software. Post-processing of binary files was done with EdiRe (University of Edinburgh, Scotland). Additional details are provided in Diongue et al. (2022).

2.3.2 | Stable isotopes analyses

Oxygen and hydrogen isotope ratios of bulk soil waters were determined from soil samples, using the water-vapour equilibration method described by Wassenaar et al. (2008). To detect any water loss that might have occurred during sample preparation, the samples in their respective Ziploc bags were weighed upon arrival at the laboratory, and again before and after analysis. No water loss was observed. Bags were inflated with dry air and left for 3 days to reach equilibrium. The isotope ratios of the vapour were determined using a laser-based isotope analyser (Picarro L2130-i). Isotope ratios of the bulk soil water samples were calculated from calibrations that were based upon isotopic internal standard samples (see below), all of which were identically prepared and analysed. Per the Laboratory's protocol, internal standard samples were run after every three of our samples. The headspace vapour was sampled for approximately 4–5 min, and the final 60 sec of the δ^2H and $\delta^{18}O$ readings were averaged. The standard deviations for $\delta^{18}O$ and δ^2H were less than 0.5‰ and 1.0‰, respectively.

To determine the oxygen and hydrogen isotope ratios of liquid (precipitation and groundwater) samples, the Laboratory used a (Picarro L2140-i) laser-based isotope analyser. The laboratory used a two-point calibration against the Laboratory's reference standard samples (deionized Baltic Sea water and tap water) that are themselves calibrated twice a year against international standards (Vienna Standard Mean Ocean Water (VSMOW), and the U. S. Geological Survey (USGS) standards USGS 46, USGS 47, and USGS 50). Each of our liquid samples was analysed up to seven times. The precision of these analyses was better than 0.1 ‰ for $\delta^{18}O$, and better than 0.5 ‰ for δ^2H .

Stable isotope ratios of all samples (expressed in ‰ units relative to the VSMOW) were calculated using Equation (1). When calculating $\delta^{18}O$, R_{sample} is the $^{18}O/^{16}O$ ratio of the sample, and R_{standard} is the $^{18}O/^{16}O$ ratio of the VSMOW. For δ^2H , R_{sample} represents the sample's $^2H/^1H$ ratio, and R_{standard} is the $^2H/^1H$ ratio of the VSMOW.

$$\delta(\text{‰}) = \frac{R_{\text{sample}} - R_{\text{standard}}}{R_{\text{standard}}} \times 1000. \quad (1)$$

2.4 | Quantification of water fluxes

2.4.1 | Evaporation

Evaporation losses (E_a) from the unsaturated soil profiles were quantified using the steady-state isothermal evaporation model developed by Allison and Barnes (1983):

$$E_a = (1 - ha) N_{sat} \tau D^v \frac{(p - WWC)}{\rho_w z_{ef}}, \quad (2)$$

$$D^v = 2.25 \times 10^{-5} \times \left(\frac{T}{273.15} \right)^{1.8}, \quad (3)$$

where ha (–) is the relative humidity; N_{sat} is the saturated water vapour density (kg m^{-3}); τ is the tortuosity (estimated by Penman (1940) as 0.67 for sandy soil); p (–) is the porosity; z_{ef} (m) is the depth of the evaporation front (defined as the depth of the highest δ -values in the profile); D^v ($\text{m}^2 \text{s}^{-1}$) is the diffusivity of water vapour in the air (calculated from the empirical function obtained from Marrero and Mason 1972); and T ($^{\circ}\text{C}$) is the air temperature.

2.4.2 | Evapotranspiration partitioning

We used the two mass-balance equations that follow (developed by Sutanto et al. (2012) and Liebhard et al. (2022)) to compute the partitioning of ET_a between soil evaporation (E_a) and transpiration (T_a , by groundnut crops or pasture). The E_a and T_a rates obtained via these mass balances are averages for a given time interval. The subscript i denotes values at the beginning of the interval, and the subscript f denotes values at the end.

$$m_i + m_p = m_{total} = m_e + m_f + m_t + m_l, \quad (4)$$

$$\delta_i x_i + \delta_p x_p = \delta_e x_e + \delta_f x_f + \delta_t x_t + \delta_l x_l. \quad (5)$$

In Equation (4), each m represents the mass of water (normalized per unit volume of soil in the sampled profile) that corresponds to a particular component of the mass balance. Specifically, m_i and m_f are, respectively, the initial and final amounts of water stored within the soil; p is the amount of precipitation during the time interval; e is the loss due to evaporation; t is the loss due to transpiration; and l is the loss due to percolation. In Equation (5), each x_k is the fraction of total water that corresponds to component k . For example, $x_p = m_p/m_{total}$. When used to calculate mass balances on ^{18}O , each δ_k in Equation (5) represents component k 's value of $\delta^{18}\text{O}$. The same δ_k 's represent the components' respective values of $\delta^2\text{H}$ when calculating mass balances on Deuterium.

In the present research, the factors δ_i , x_i , δ_p , x_p , δ_f , x_f , δ_l , and x_l were obtained from measurements. As detailed below, the δ_i and δ_f for the isotopes in a given soil-profile are weighted means for the soil water in those samples. δ_p is the weighted mean of precipitation; and

δ_j is the ratio of the sample at the bottom of the soil-profile. The data used to calculate the δ_e were (i) the fractionation factor ϵ_{total} (see below), and (ii) the value of δ that was present at the soil surface (5 cm depth). δ_t was calculated from a combination of the weighted mean of δ , the soil volumetric water content (VWC), and the root-length density (RD) of soil layer j (see Liebhard et al., 2022):

$$\delta_i = \delta_f = \frac{\sum_{j=1}^n \delta_j (VWC_j H_j)}{\sum_{j=1}^n (VWC_j H_j)}, \quad (6)$$

$$\delta_t = \frac{\sum_{j=1}^n \delta_j (VWC_j H_j RD_j)}{\sum_{j=1}^n (VWC_j H_j RD_j)}, \quad (7)$$

$$\delta_e = \delta_{surface} - \epsilon_{total}. \quad (8)$$

Following Dongmann et al. (1974), each isotope's overall fractionation by evaporation (ϵ_{total}) was calculated as the sum of the isotope's equilibrium fractionation between liquid water and water vapour (ϵ_{eq}), and its kinetic fractionation (ϵ_k). The values of ϵ_{eq} were computed per Horita and Wesolowski (1994):

$$\epsilon_{eq} = (\alpha^+ - 1) 10^3 (\text{‰}), \quad (9)$$

$$10^3 \ln [\alpha^+ (2H)] = 1158.8 \left(\frac{T^3}{T^9} \right) - 1620.1 \left(\frac{T^2}{T^6} \right) + 794.84 \left(\frac{T}{T^3} \right) - 161.04 + 2.9992 \left(\frac{10^9}{T^3} \right), \quad (10)$$

$$10^3 \ln [\alpha^+ (^{18}\text{O})] = -7.685 + 6.7123 \left(\frac{10^3}{T} \right) - 1.6664 \left(\frac{10^6}{T} \right) + 0.3504 \left(\frac{10^9}{T^3} \right), \quad (11)$$

where α^+ is the difference between the isotopic compositions of liquid and vapour phases at isotopic equilibrium, and T (K) is the air temperature.

The kinetic fractionation ϵ_k quantifies isotopic effects during net evaporation, and results from the higher diffusivities of isotopically lighter molecules. It was estimated following Gat (1996) and Horita et al. (2008):

$$\epsilon_k = \theta n (1 - h) \left(1 - \frac{D_i}{D} \right) 10^3 (\text{‰}), \quad (12)$$

where θ is close to unity for soil water and small water bodies (Gat, 1996). The factor n accounts for the aerodynamic regime above the evaporating liquid-vapour interface, and is assumed to equal one

for fully diffusive transport, as is appropriate for dry soil conditions (Benettin et al., 2018). h (–) is the relative humidity of the air overlying the evaporating surface. The term D_i/D is the ratio between the diffusivities of the heavy and light isotopes. Per Merlivat (1978), the commonly accepted values for D_i/D of ^2H and ^{18}O are 0.9755 and 0.9723, respectively.

Under the assumptions that they described in their respective works, Sutanto et al. (2012) and Liebhard et al. (2022) determined x_t and x_e as residuals of the mass balances that are given in Equations (4) and (5):

$$x_t = x_p + x_i - x_e - x_f - x_l, \quad (13)$$

$$x_e = \frac{(\delta_i x_i + \delta_p x_p - \delta_f x_f - \delta_l x_l - \delta_t x_t + \delta_i x_t + \delta_l x_t - \delta_i x_i)}{(\delta_e - \delta_t)}. \quad (14)$$

As noted earlier, the present study computed mass balances based on both $\delta^2\text{H}$ and $\delta^{18}\text{O}$. The results are reported as the mean and standard deviation. Data from isotope profiles down to a depth of 100 cm were used to cover the entire root zone of groundnut (at Site 1) and pasture (at Site 2). It is essential to consider the whole root zone because δ_t was weighted with the root-length density (see Equation 7). For groundnut crops, 72.4% of the root system was within the 0–20 cm soil layer depth, while 27.6% was found at 20–50 cm depth (Siegwart et al., 2022). Root-length density in the pasture at Site 2 was assumed to decrease linearly from its maximum value at the soil surface down to its minimum at the maximum root length (around 40 cm, according to Glendening (1941)). Rainfall amounts were measured at both sites with a weather station (Campbell TE25MM at Site 1, and Campbell Climavue 50TM at Site 2). Values for the soil-water storage (m_i and m_f in Equation 4) were derived from the VWC of each soil profile, and ET_a was estimated from eddy covariance fluxes at Site 1 (Diongue et al., 2022). For that site, the only unknown variable in the mass balance was the percolation, which was calculated as the residual from the water balance equation (Equation 4). Percolation at Site 2 could not be estimated because the ET_a was unknown. Therefore, percolation at that site was assumed to negligible due to the low level of water storage in the soil (Moriana et al., 2003; Nielsen & Vigil, 2010).

2.4.3 | Groundwater recharge

The groundwater recharge rates (R in mm y^{-1}) were estimated by applying the piston displacement method (Allison et al., 1983) to data from deep soil samples (>150 cm; see Figure 3). The method is based upon a simple empirical relationship. As given in Clark and Fritz (1997), the relationships for $\delta^2\text{H}$ and $\delta^{18}\text{O}$ are

$$R = \left(\frac{22}{\delta^2 H_{\text{shift}}} \right)^2, \quad (15)$$

$$R = \left(\frac{3}{\delta^2 O_{\text{shift}}} \right)^2. \quad (16)$$

where $\delta^2 H_{\text{shift}}$ is the difference between (i) the deuterium excess of the local meteoric water line (LMWL), and (ii) the intercept of the linear regression for isotope data from deep soil samples.

We used soil data from Site 1 to assess the relevance of the piston displacement method and to quantify the annual groundwater recharge of the CT aquifer. We could not estimate the groundwater recharge for Site 2, because the groundwater table is at 50–70 m depth, and our soil profiles extended down to only 300 cm. Nor were any wells or boreholes available for sampling the CT at that location.

2.5 | Further data analysis

To assess the influence depth of isotope fractionation, the line-conditioned excess (*lc-excess*; Landwehr & Coplen, 2006) was calculated for each soil sample:

$$lc - excess = \delta^2 H - a \times \delta^{18} O - b, \quad (17)$$

where a and b are, respectively, the slope and intercept of the LMWL. The *lc-excess* expresses the degree to which the $\delta^2\text{H}$ of the sample deviates from the LMWL. The physical significance of that deviation is that non-equilibrium, dynamic fractionation has been caused by evaporation. Larger negative values indicate larger evaporative losses.

An additional analysis was used to evaluate whether the different slope locations at each site differed significantly in their values of E_a , T_a , and R . For this purpose, we used the non-parametric Kruskal–Wallis test with Wilcoxon pair-wise comparisons, and $p = 0.05$. The same test was used to evaluate the differences between E_a , T_a , and R for the two canopy covers at Site 1.

3 | RESULTS

3.1 | Isotopic composition of rainfall, soil water, and groundwater

Figure 2 presents dual-isotope plots for the two sites' rainfall, soil water, and groundwater. At Site 1, the $\delta^2\text{H}$ of rainfall ranged from -79.5‰ to 3.5‰ , and the $\delta^{18}\text{O}$ varied from -11.1 to -0.1‰ . In contrast, the ranges for rainfall at Site 2 were $-91.0 \leq \delta^2\text{H} \leq -5.1\text{‰}$, and $-12.5 \leq \delta^{18}\text{O} \leq -1.2\text{‰}$. The LMWL at Site 1 was $\delta^2\text{H} = 7.61 \pm 0.20 \times \delta^{18}\text{O} + 7.50 \pm 1.23$ ($R^2 = 0.98$), versus $\delta^2\text{H} = 7.48 \pm 0.22 \times \delta^{18}\text{O} + 6.8 \pm 1.3$ ($R^2 = 0.98$) for Site 2. Both of these lines, whose slopes and intercepts were calculated via an amount-weighted regression, are lower than the global meteoric water line (GMWL: $\delta^2\text{H} = 8 \times \delta^{18}\text{O} + 10$). This finding indicates that the isotopic composition of rainfall was affected by the local climate's characteristic low relative humidity and small amounts of rainfall.

At both sites, the heavy-isotope enrichment in the soil water (unsaturated zone) is higher than in the local rainfall. (See marginal box plots in Figure 2). Most of the data for soil water fall below the sites' respective LMWLs. More specifically, at both sites the slopes and intercepts of the soil-water regression lines are lower than those

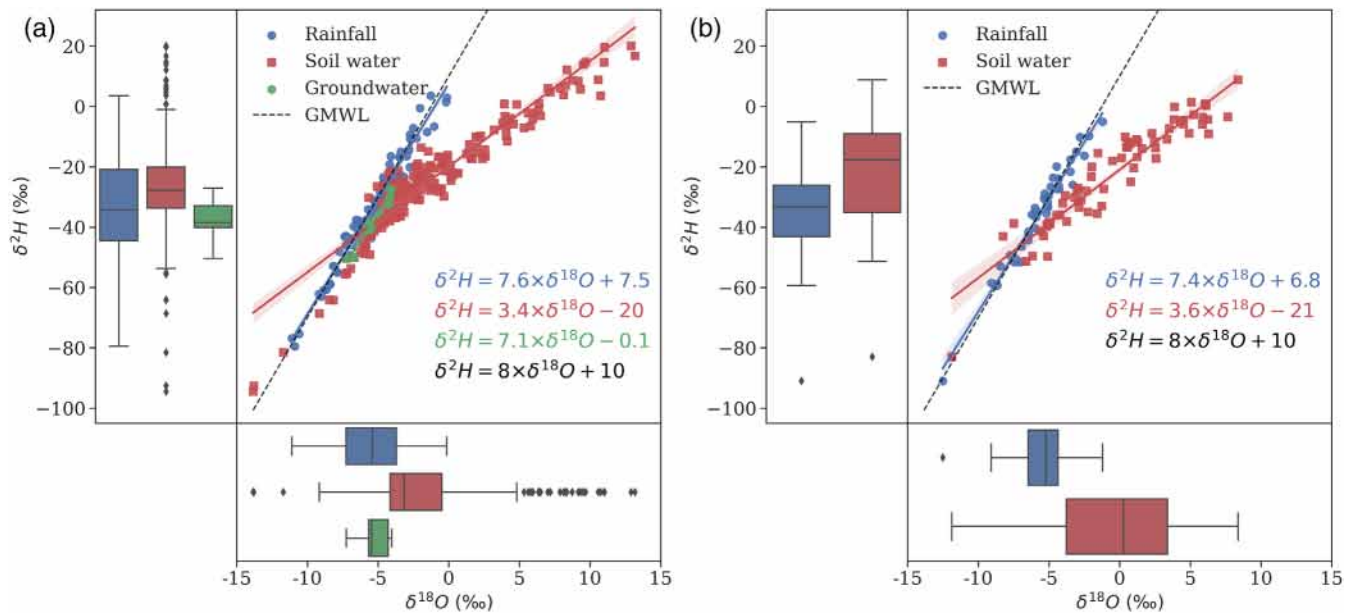


FIGURE 2 Dual stable isotope and marginal box plots for rainfall (blue circle), soil water (red square) and groundwater (green hexagon) at (a) site 1 (groundnut basin) and (b) site 2 (Ferlo Valley). Also presented are the GMWL (dark dashed line); regression lines (coloured, with shading to show the standard deviation); and the equations for rainfall (LMWLs), soil water, and groundwater.

of the LMWL. At Site 1, the line for soil water is $\delta^2\text{H} = 3.4 \times \delta^{18}\text{O} - 20$, versus $\delta^2\text{H} = 7.6 \times \delta^{18}\text{O} + 7.5$ for the LMWL, while at Site 2, the soil-water line and LMWL are (respectively) $\delta^2\text{H} = 3.6 \times \delta^{18}\text{O} - 21$ and $\delta^2\text{H} = 7.4 \times \delta^{18}\text{O} + 6.8$. This result indicates (i) that at both sites, rainfall is the main source of soil water, and (ii) that the degree of evaporation experienced by soil water differs from that of the rainfall. Data for groundwater samples at Site 1 plot close to the LMWL, but with a lower slope (7.1) and intercept (-0.17), suggesting that the CT aquifer is recharged by modern precipitation, which is affected little by evaporation processes prior to rainfall infiltration and/or during soil water percolation. Note that the data for some of the Site 1 soil-water samples plot along with the groundwater samples, perhaps because the soil water was influenced by the capillary fringe.

3.2 | Spatiotemporal variability of bulk soil water isotopic composition

3.2.1 | Site 1

Figure 3 displays the $\delta^{18}\text{O}$, lc -excess, and VWC in upper-slope profiles, under and outside of tree canopies, as a function of depth and sampling period. (Profiles for mid-slope and lower-slope locations are in the supplementary materials; Figures S1 and S2). $\delta^2\text{H}$ is not shown because its distribution is similar to that of $\delta^{18}\text{O}$. Any differences between these distributions are expressed indirectly by the lc -excess.

The isotopic ratios in the deeper soil zone are mostly constant in all profiles regardless the slope location, canopy cover, or season. The mean $\delta^{18}\text{O}$ values (which range between -2.8‰ and -4.4‰) are similar to that of the groundwater (-5.27‰), except in lower-slope

locations outside of the canopy, where the soil water is more depleted in heavy isotopes ($\delta^{18}\text{O} = -9.0\text{‰}$).

The $\delta^{18}\text{O}$ in the upper soil form a distinct pattern, which is essentially the same under canopies as outside of them. During the dry season (February, June, and December), ratios in the 15–40 cm depth range are high. Then, they decrease exponentially with depth down to the bottom of the shallow soil-water zone (at 150 cm), after which they are essentially constant from 150 cm down to 500 cm. In contrast, during the wet season the $\delta^{18}\text{O}$ ratios are essentially constant from the surface all the way down to 500 cm. This seasonal difference is attributable to the competing effects of evaporation and rainfall-infiltration. During the dry season, evaporation causes soil water in the upper 15 cm to become enriched in heavy isotopes. The influence of evaporation decreases with depth, thereby leading to the observed exponential decrease in $\delta^{18}\text{O}$ ratios. In contrast, percolation of rainfall during the wet season maintains the ratios almost constant from the surface down to 500 cm.

The depth intervals with the highest $\delta^{18}\text{O}$ values also have the lowest (i.e., most-negative) lc -excess values (Figures 2b). The depth at which these values occur is defined as the evaporation front. It marks the transition zone above which diffusion of water vapour dominates movement of liquid water. During the dry season, the lc -excess at the evaporation front varied from -91.2‰ to -60.2‰ . The lowest values occurred mainly in open areas (i.e., outside of the canopy). These low lc -excess values indicate that evaporation losses are high during the dry season. During the wet season (August), the mean $\delta^{18}\text{O}$ value at the upper soil surface (-5.03‰) is similar to the amount-weighted mean of rainfall (-5.47‰), with a mean lc -excess of -9.8‰ . The lc -excess at the evaporation front diminishes with depth in all profiles except in lower-slope locations outside the canopy, where the value is -33‰ at the 50 cm depth.

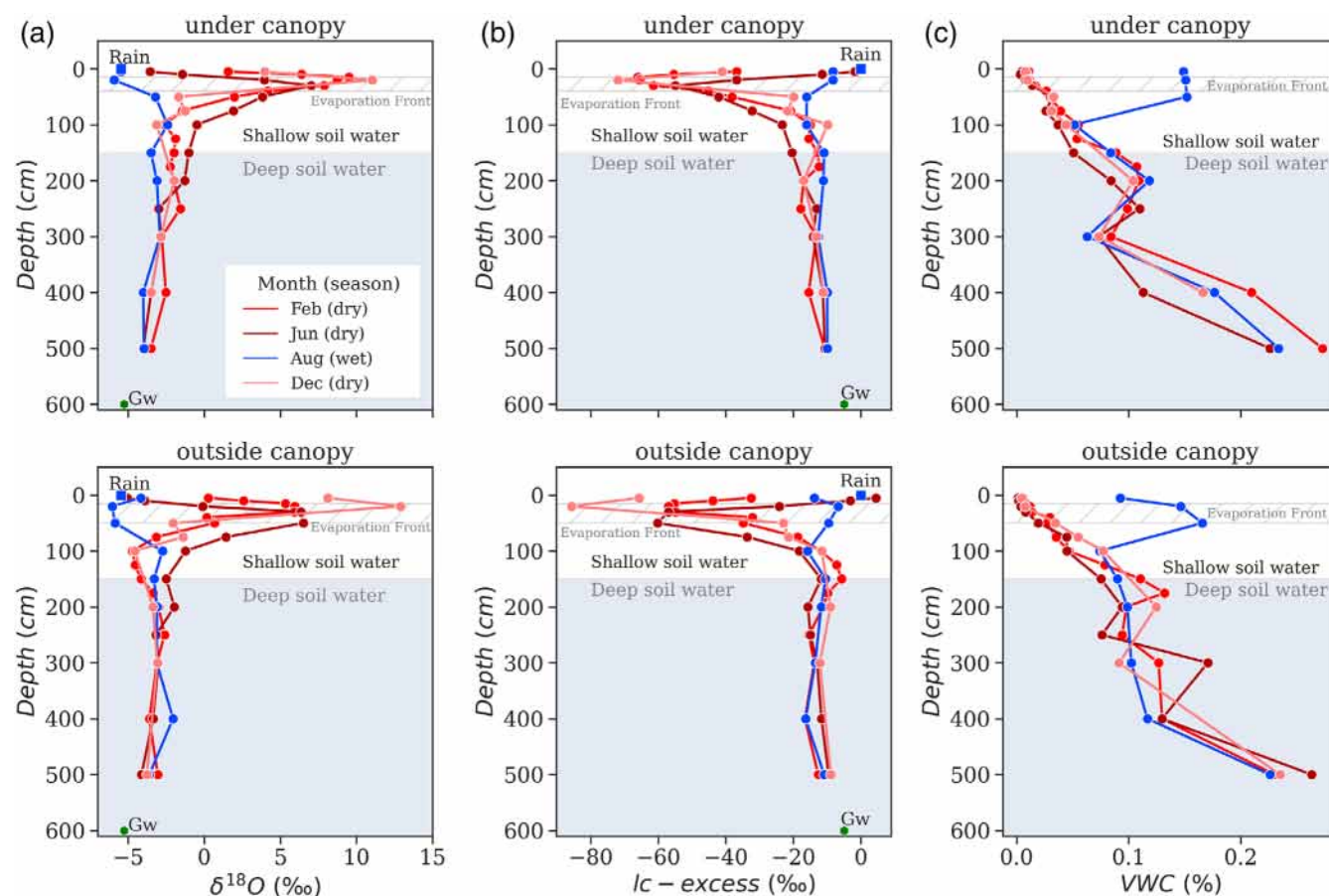


FIGURE 3 Profiles, at the upper slope location in site 1, of (a) soil water isotopic ratio ($\delta^{18}\text{O}$), (b) lc -excess, and (c) soil volumetric water content (VWC) for the indicated sampling months (seasons) under and outside the canopy of *Faidherbia albida*. (data for the other profiles are in the supplementary materials). Hatched areas indicate the evaporation-front depth intervals. Shaded grey areas represent the separation between the shallow and the deep soil water. In (a) and (b), the blue square indicates the amount-weighted mean composition of rainfall (rain) at the soil surface, and the green hexagon shows the mean isotopic composition of groundwater (Gw) at a depth of around 600 cm.

VWCs at the soil surface and in the shallow soil layer are low during the dry season, when the mean VWCs at the upper, middle, and lower slope are 2.9%, 2.0%, and 3.1%, respectively. During the wet season, rainfall infiltration increases the values at those same locations to, respectively, 11.6%, 10.8%, and 17.0%. In the deep soil layer, where VWC is less affected by seasonal variations, values at those locations tend to increase with depth down to the capillary fringe, where the values reach maximums of 28.4%, 19.2%, and 27.3%, respectively. The lower slope is the wettest (mean VWC: 16.8%), followed by the upper slope (13.8%) and the mid-slope (9.74%) (Figures S1 and S2). There is no significant difference in VWCs between the different canopy covers except in the lower slope during the wet season, when the VWC is 21.5% underneath the canopy, versus 12.5% outside of it ($p < 0.05$).

3.2.2 | Site 2

Isotopic-profile patterns at Site 2 are similar to those at Site 1 (Figure 4). $\delta^{18}\text{O}$ ratios vary with depth and season within the shallow soil water

(down to 100 cm), but are essentially constant from 100 cm down to 300 cm depth.

During the dry season, the evaporation front at the lower slope is at a shallower depth than at the mid-slope (depth = 15–30 cm at the lower slope, with lc -excess values of -67.2% and -48.5% , respectively, versus (for the mid-slope) at depths of 40–75 cm, with lc -excess values of -54.2% and -52.1%). During the wet season, when only the upper part of the profile (0–50 cm depth) was sampled, no distinct evaporation front is identifiable. The isotopic composition at the soil surface at the mid-slope (-5.10%) is similar to the weighted-mean rainfall value (-5.56%), but the soil water at the lower slope is more enriched in heavy isotopes (-2.87%).

Isotopic compositions varied considerably in the deep-soil waters, which were sampled only during the dry season (in February and June). The variation was greater at mid-slope, where the mean lc -excess values range from -26.6% to -19.9% , as compared to the almost constant values (-8.2% to -8.9%) in the lower slope. In addition, during the dry season the deep-soil water at the lower slope is more depleted in heavy isotopes (and closer to the isotopic ratios of

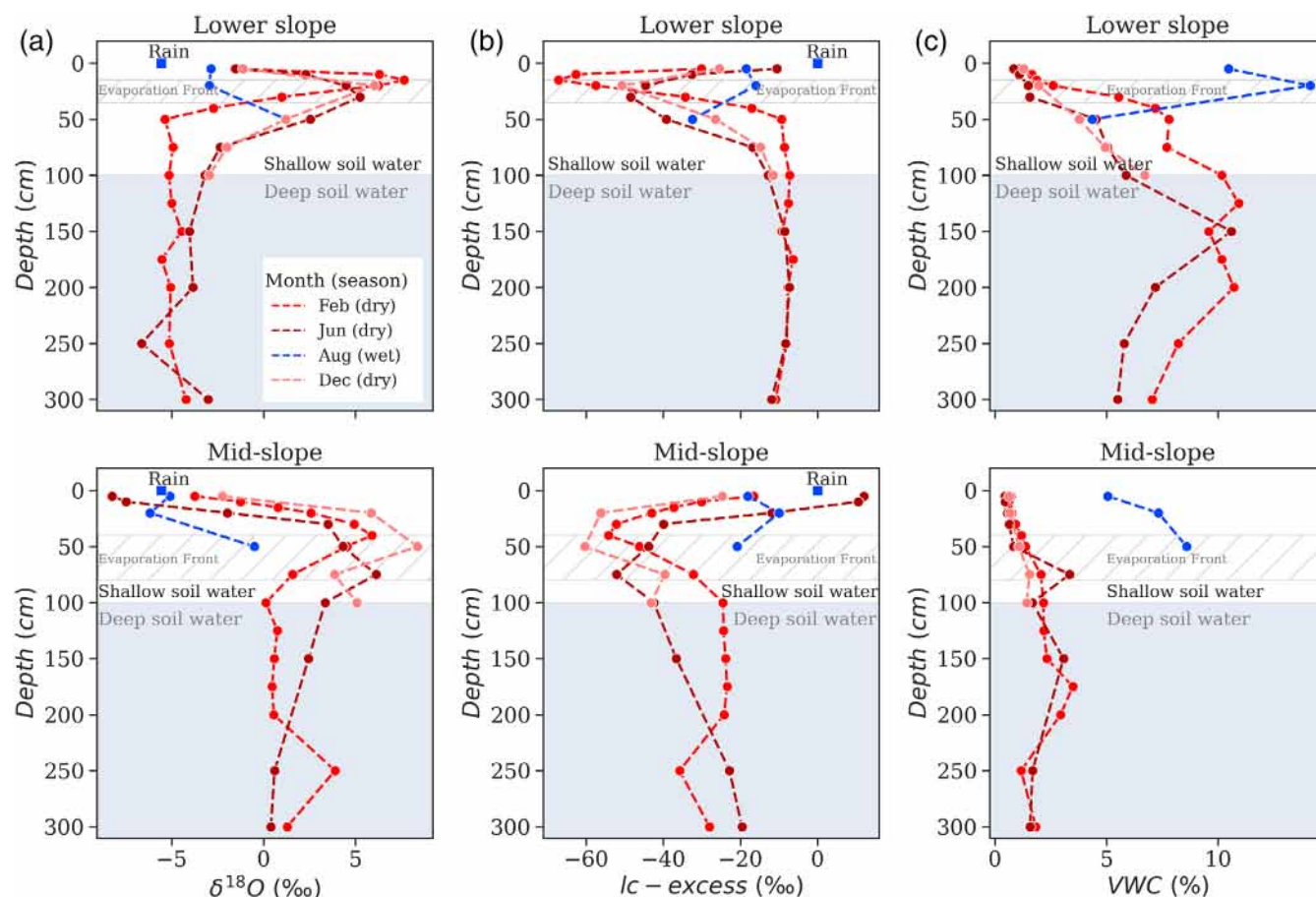


FIGURE 4 Profiles, at the lower and middle slope locations in site 2, of (a) soil water isotopic ratio ($\delta^{18}\text{O}$), (b) soil water lc -excess; and (c) soil volumetric water content (VWC) during the indicated sampling months (seasons). Hatched areas indicate the evaporation-front depth intervals. Shaded grey areas represent the separation between the shallow and the deep soil water. In (a) and (b), the blue square indicates the amount-weighted mean composition of rainfall (rain) at the soil surface.

local rainfall, -5.56‰) than at mid-slope (mean $\delta^{18}\text{O} = -4.69\text{‰}$ at the lower slope, versus -0.08‰ at the upper slope).

Soil moisture during the dry season is significantly higher ($p < 0.05$) at the low-slope location ($0.8\text{--}10.9\%$) than at the mid-slope ($0.5\text{--}3.5\%$). The vertical distribution of the VWC for the wet season is difficult to interpret because only the upper part of the profile was sampled. However, the means for the lower slope and mid-slope are similar ($p = 0.51$), at around 8.3% .

3.3 | Water fluxes

3.3.1 | Evapotranspiration

Calculation of evaporation using the isothermal evaporation model

The isothermal evaporation model developed by Allison and Barnes (1983) is used to calculate evaporation rates (E_a) from the isotope profiles of soil water. Evaporation fronts could not be identified from wet-season profiles. Rates that were calculated from dry-season data ranged from 0.02 to 0.09 mm d^{-1} at Site 1, and from 0.02 to 0.11 mm d^{-1} at Site 2.

The lowest E_a values are for June, when the VWC are the lowest (Table 1). At Site 1, mean values are similar between locations, at around 0.05 mm d^{-1} . At the upper- and mid-slope locations in Site 1, the mean E_a underneath the canopy is higher than in open areas (Figure 5), but the difference is not significant ($p = 0.34$). Estimated E_a values for Site 2 indicate that more evaporation takes place at the lower slope ($0.08 \pm 0.03\text{ mm d}^{-1}$) than at the mid-slope ($0.04 \pm 0.01\text{ mm d}^{-1}$). Again, the difference is not significant ($p = 0.121$). However, lc -excess values confirm that evaporation is higher at the lower slope.

Evaporation and transpiration partitioning for the groundnut crop (Site 1) and pasture (Site 2)

The isotope mass balance approach (Section 2.4.2) was used to calculate this partitioning. The times (and corresponding field conditions) during which we ran this calculation were: (i) February–June (bare soil, no crop and pasture); (ii) June–August (initial growing stage); and (iii) August–December (vegetative growing stage and harvesting). Table 2 summarizes the parameters and $\delta^{18}\text{O}$ isotope profiles used in the mass balance. (Parameters for $\delta^2\text{H}$ are presented in the

TABLE 1 Parameters used for estimating evaporation rates (E_a) via equation 5 for sites 1 and 2 at different slope locations during the three evaluation periods. z_{ef} is the depth of the evaporation front (i.e., where $\delta^{18}\text{O}$ is highest, and lc -excess values are lowest); WVC is the weighted mean of the soil volumetric water content in the shallow soil; and h_a and T are, respectively, the relative humidity and air temperature. D^v (the diffusivity of water vapour in the air) is a function of T .

Date	Station	z_{ef} (cm)	$\delta^{18}\text{O}$ (‰)	Lc-excess (‰)	WVC (%)	h_a (%)	T (°C)	D^v ($\text{m}^2 \text{s}^{-1}$)	E_a (mm d^{-1})
<i>Site 1 (Groundnut Basin)—under the canopy</i>									
17/02/2021	Mid-slope	20	8.36	−59.14	3.55	0.23	27.4	3.58 E-05	0.073
18/02/2021	Upper slope	15	9.51	−66.05	4.56	0.27	27.2	3.55 E-05	0.088
03/06/2021	Upper slope	30	7.02	−54.92	3.33	0.5	29.5	4.09 E-05	0.038
04/06/2021	Lower Slope	30	5.62	−52.52	6.48	0.45	31.2	4.52 E-05	0.042
05/06/2021	Mid-slope	20	4.35	−44.49	2.88	0.55	29.4	4.07 E-05	0.05
10/12/2021	Lower Slope	20	9.17	−69.02	4.99	0.24	26.4	3.35 E-05	0.064
10/12/2021	Mid-slope	20	9.69	−66.52	4.19	0.24	26.4	3.35 E-05	0.066
10/12/2021	Upper slope	20	11.03	−71.91	3.06	0.24	26.4	3.35 E-05	0.068
<i>Site 1 (Groundnut Basin)—outside the canopy</i>									
17/02/2021	Mid-slope	30	13.18	−91.19	2.05	0.23	27.4	3.58 E-05	0.054
18/02/2021	Upper slope	30	5.93	−54.87	5.08	0.27	27.2	3.55 E-05	0.045
03/06/2021	Upper slope	30	6.34	−56.93	4.34	0.5	29.5	4.09 E-05	0.037
04/06/2021	Lower Slope	30	4.18	−43.68	5.84	0.45	31.2	4.52 E-05	0.043
05/06/2021	Mid-slope	50	5.79	−58.15	1.91	0.55	29.4	4.07 E-05	0.022
10/12/2021	Lower Slope	20	10.74	−85.79	1.88	0.24	26.4	3.35 E-05	0.071
10/12/2021	Mid-slope	20	10.99	−76.66	1.72	0.24	26.4	3.35 E-05	0.072
10/12/2021	Upper slope	20	12.9	−85.68	4.48	0.24	26.4	3.35 E-05	0.065
<i>Site 2 (Ferlo)</i>									
18/02/2021	Lower slope	15	7.65	−67.2	8.01	0.2	29.1	3.99 E-05	0.117
18/02/2021	Mid-slope	40	5.89	−54.22	1.78	0.2	29.1	3.99 E-05	0.051
06/06/2021	Lower slope	30	5.25	−48.51	6.23	0.42	30	4.22 E-05	0.048
06/06/2021	Mid-slope	75	6.13	−52.12	2.08	0.42	30	4.22 E-05	0.021
11/12/2021	Lower slope	20	6.03	−50.76	4.41	0.14	27	3.49 E-05	0.092
11/12/2021	Mid-slope	50	8.37	−60.36	1.2	0.14	27	3.49 E-05	0.039

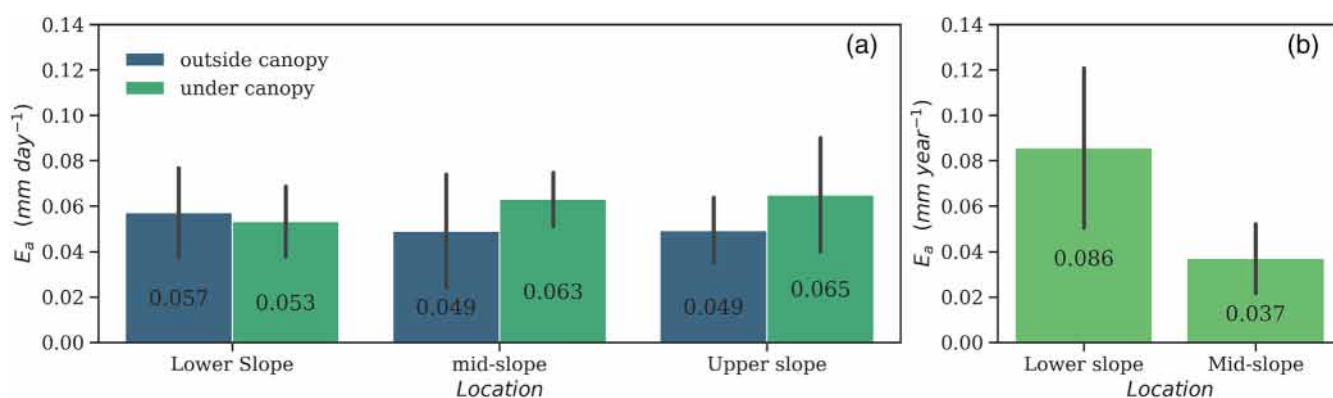


FIGURE 5 Mean steady-state evaporation losses at (a) site 1 (under and outside the tree canopy) and (b) site 2. Error bars show the standard deviations associated with the three sampling periods (Feb, Jun, and Dec).

supplementary material, Table S2). Figure 6 displays the mean values of E_a and T_a rates obtained by using $\delta^{18}\text{O}$ and $\delta^2\text{H}$ isotope data separately. The standard deviation of these rates is less than 0.25 and 0.27 mm d^{-1} for E_a and T_a rates, respectively, during all evaluation periods at both sites.

Because crops at Site 1 are rainfed, the soil is bare during the dry season (February to June). Therefore, soil evaporation is the main component of water loss. During this period, evaporation varies underneath and outside the canopy cover from 0.03 to 0.01 mm d^{-1} on the mid-slope, and from 0.05 to 0.06 mm d^{-1} on the upper slope.

TABLE 2 Summary of the mass balances for water and isotopes in the top 100 cm of soil profiles at Sites 1 and 2 during the three evaluation periods. N is the number of days between two consecutive sampling periods. VWC is the soil water storage; δ is $\delta^{18}\text{O}$, rain is the rainfall amount; ET_a is the actual evapotranspiration (from eddy-covariance fluxes); and Q is the percolation. The subscripts i and f indicate, respectively, values at the beginning and end of the time interval between samplings. p is precipitation, e is evaporation, t is transpiration, and q is percolation. ET_a and Q were not available at Site 2. Due to low soil water storage at that site, percolation there was assumed to be insignificant for the purposes of the isotope mass balance.

Sampling	N (day)	Location	VWC_i (mm)	δ_i (‰)	VWC_f (mm)	δ_f (‰)	Rain (mm d ⁻¹)	δ_p (‰)	ET_a (mm d ⁻¹)	δ_e (‰)	δ_t (‰)	Q (mm d ⁻¹)	δ_q (‰)
<i>Groundnut crops under canopy cover (Site 1)</i>													
Feb-Jun	105	Mid-slope	31.4	-1.4	26.5	-0.3	0.00	-7.4	0.17	-19.5	-1.7	0.00	-4.1
Feb-Jun	105	Upper slope	32.8	-0.2	24.7	2.2	0.00	-7.4	0.17	-17.6	-0.7	0.00	-2.6
Jun-Aug	68	Lower slope	38.2	-1.4	207.2	-5.6	2.68	-4.9	1.39	-18.5	-1.4	0.00	-3.2
Jun-Aug	68	Mid-slope	26.5	-0.7	124	-5.0	2.68	-4.9	1.39	-16.3	-0.9	0.00	-2.7
Jun-Aug	68	Upper slope	24.7	1.8	101.3	-3.9	2.68	-4.9	1.39	-17.9	1.8	0.16	-0.5
Aug-Dec	121	Lower slope	207.2	-5.5	49.9	-2.1	2.48	-7.2	2.66	-19.6	-5.3	1.12	-5.1
Aug-Dec	121	Mid-slope	124.0	-4.6	41.9	-3.1	2.48	-7.2	2.66	-19.4	-4.4	0.50	-2.3
Aug-Dec	121	Upper slope	101.3	-3.8	30.6	-1.1	2.48	-7.2	2.66	-19.6	-2.9	0.40	-2.4
<i>Groundnut crops outside canopy cover (Site 1)</i>													
Feb-Jun	105	Mid-slope	15.3	1.5	14.8	2.2	0.00	-7.4	0.17	-22.9	1.4	0.00	-0.8
Feb-Jun	105	Upper slope	29.0	-2.3	27.5	1.1	0.00	-7.4	0.17	-18.9	-2.6	0.00	-4.7
Jun-Aug	68	Lower slope	29.6	-0.2	104.2	-3.0	2.68	-4.9	1.39	-18.6	-0.2	0.19	-2.2
Jun-Aug	68	Mid-slope	14.8	2.2	115	-4.6	2.68	-4.9	1.39	-20	2.4	0.00	-0.1
Jun-Aug	68	Upper slope	27.5	1.1	113.4	-4.8	2.68	-4.9	1.39	-19.4	1.2	0.02	-1.2
Aug-Dec	121	Lower slope	104.2	-3	18.8	0.4	2.48	-7.2	2.66	-17.9	-1.8	0.53	-4.2
Aug-Dec	121	Mid-slope	115.0	-4.6	17.2	-0.1	2.48	-7.2	2.66	-20.2	-4.6	0.63	-3
Aug-Dec	121	Upper slope	113.4	-4.8	44.8	-2.5	2.48	-7.2	2.66	-18.3	-4.5	0.39	-2.8
<i>Pasture (Site 2)</i>													
Feb-Jun	105	Low slope	68.9	-3.8	40.4	-0.9	0.00	-	-	-21.4	-3.38	-	-5.1
Feb-Jun	105	Mid-slope	15.4	1.7	15.9	4.4	0.00	-	-	-11.5	2.11	-	-1.3
Jun-Aug	68	Low slope	40.4	-0.9	39.5	-1.6	1.23	-6.9	-	-17.5	-0.42	-	2.5
Jun-Aug	68	Mid-slope	15.9	4.4	39.3	-2.4	1.23	-6.9	-	-22.5	4.44	-	3.4
Aug-Dec	121	Low slope	39.5	-1.6	44.1	-1.0	1.62	-5.5	-	-18.6	-1.53	-	1.2
Aug-Dec	121	Mid-slope	39.3	-2.4	12	5.4	1.62	-5.5	-	-21.9	-2.42	-	-5.1

(The lower slope was not sampled in February.) The higher evaporation values recorded on the upper slope can be explained by the difference in soil water storage, which was higher for the upper-slope location (Table 2). Between June and August, cumulative rainfall is 182 mm, and the groundnut crops are in their first stage of development (seeding and budding). Therefore, T_a becomes the main component of water losses, and increases from 0.55 mm d⁻¹ at the lower slope to 1.25 mm d⁻¹ at the upper slope. T_a rates are similar regardless of the canopy cover, except at the lower slope ($p < 0.05$), where they are higher outside of the canopy cover (1.14 mm d⁻¹) than underneath it (0.55 mm d⁻¹). During this same period, the mean soil evaporation is 0–0.32 mm d⁻¹. The evaporation rate of 0 mm d⁻¹ that was obtained for February–June at the lower slope underneath the canopy is due to a negative evaporation fraction in the mass balance for this period at this location. The August to December period

corresponds to the stage of crop maturity and harvesting, when T_a (which ranges from 1.96 to 2.24 mm d⁻¹) exceeds soil evaporation (0.37–0.69 mm d⁻¹).

A similar pattern is found for pasture at Site 2. E_a is the only component of water loss during the dry season (February–June), and is greater at the lower slope (0.16 mm d⁻¹) than at mid-slope (0.02 mm d⁻¹). The difference is due to lower soil-water storage at mid-slope (mean: 15.6 mm) than at the lower slope (54.5 mm). From June to August, E_a rates are, respectively, 0.35 and 0.39 mm d⁻¹ at mid-slope and lower slope—on the same order of magnitude as values found at Site 1 during that period. However, the transpiration rate at Site 2 during this period (0.57–0.9 mm d⁻¹) is lower than in Site 1's groundnut fields. During the succeeding evaluation period (August–December), T_a rates are higher (1.30–1.63 mm d⁻¹) and E_a rates are lower (0.18–0.25 mm d⁻¹).

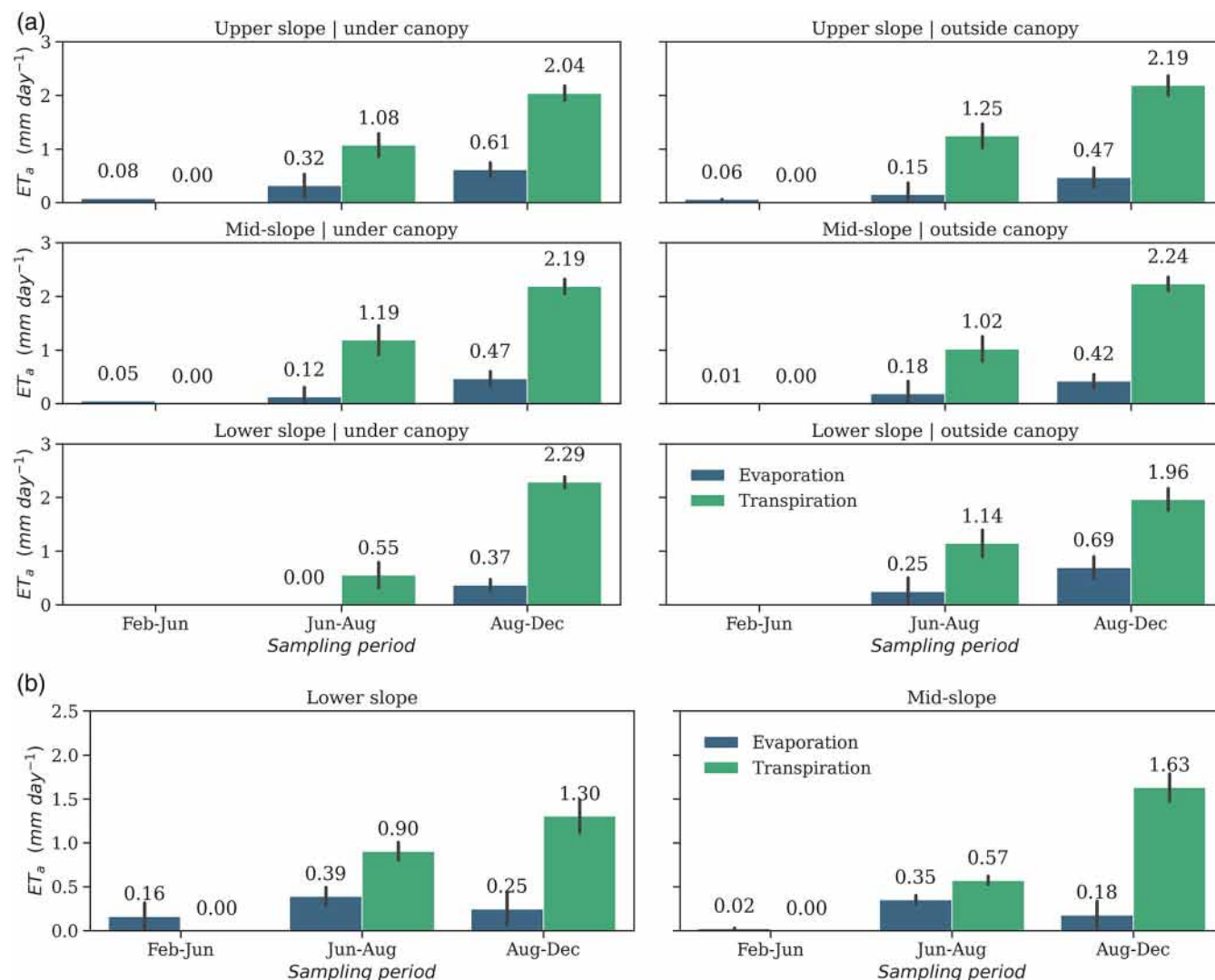


FIGURE 6 Daily evaporation and transpiration rates during the three evaluation periods for (a) groundnut crops at site 1 and (b) pasture at site 2. The error bars show the standard deviation using $\delta^{18}\text{O}$ and $\delta^2\text{H}$ separately for the mass balance calculations.

3.3.2 | Groundwater recharge based on piston displacement method

Figure 7 presents dual plots of $\delta^{18}\text{O}$ and $\delta^2\text{H}$ for soil samples collected on the upper slope at Site 1. (Plots for mid-slope and lower slope are in the supplementary materials, Figures S3 and S4). As predicted by Allison et al. (1983), data for samples from the near-surface soil (which extends downward from the evaporation front to the depth at which the $\delta^{18}\text{O}$ is nearly constant) plot along straight evaporation lines. Their slopes (from linear regression) are 2.3–3.6. Data for samples of deep soil water plot below the LMWL. The regression-line slopes for those samples range from 4.6 to 7.8, and were adjusted to that of the LMWL ($=7.61$) to force application of the model.

Figure 8 displays the mean annual recharge (calculated via both empirical relationships, see Equations (15) and (16)) and its standard deviation for each slope location and canopy cover. Values of $\delta^2\text{H}_{\text{shift}}$ and $\delta^{18}\text{O}_{\text{shift}}$ for the soil profiles that were used in the recharge estimations are presented in the supplementary materials (Table S3).

Standard deviations of the recharge estimates ranged from 0.1 to 1.4 mm y^{-1} .

The estimated recharge rates are less than 2% of annual rainfall. The difference between recharge rates under canopy and in open ground is not significant ($p = 0.8$). In contrast, the estimated recharge is significantly lower ($p = 0.032$) at the upper slope than at the mid-slope and lower slope. Specifically, the $\delta^2\text{H}_{\text{shift}}$ -based mean at the upper slope is 3.37 mm y^{-1} , versus 3.57 mm y^{-1} according to the $\delta^{18}\text{O}_{\text{shift}}$ -based calculation. The same means for the mid-slope are, respectively, 6.47 and 6.83 mm y^{-1} . At the lower slope, the means are 6.16 and 7.02 mm y^{-1} .

4 | DISCUSSION

4.1 | Isotopic composition of rainfall at the two sites

The differences between the sites' LMWLs appear to reflect differences between the sites' local climates, and possibly between their

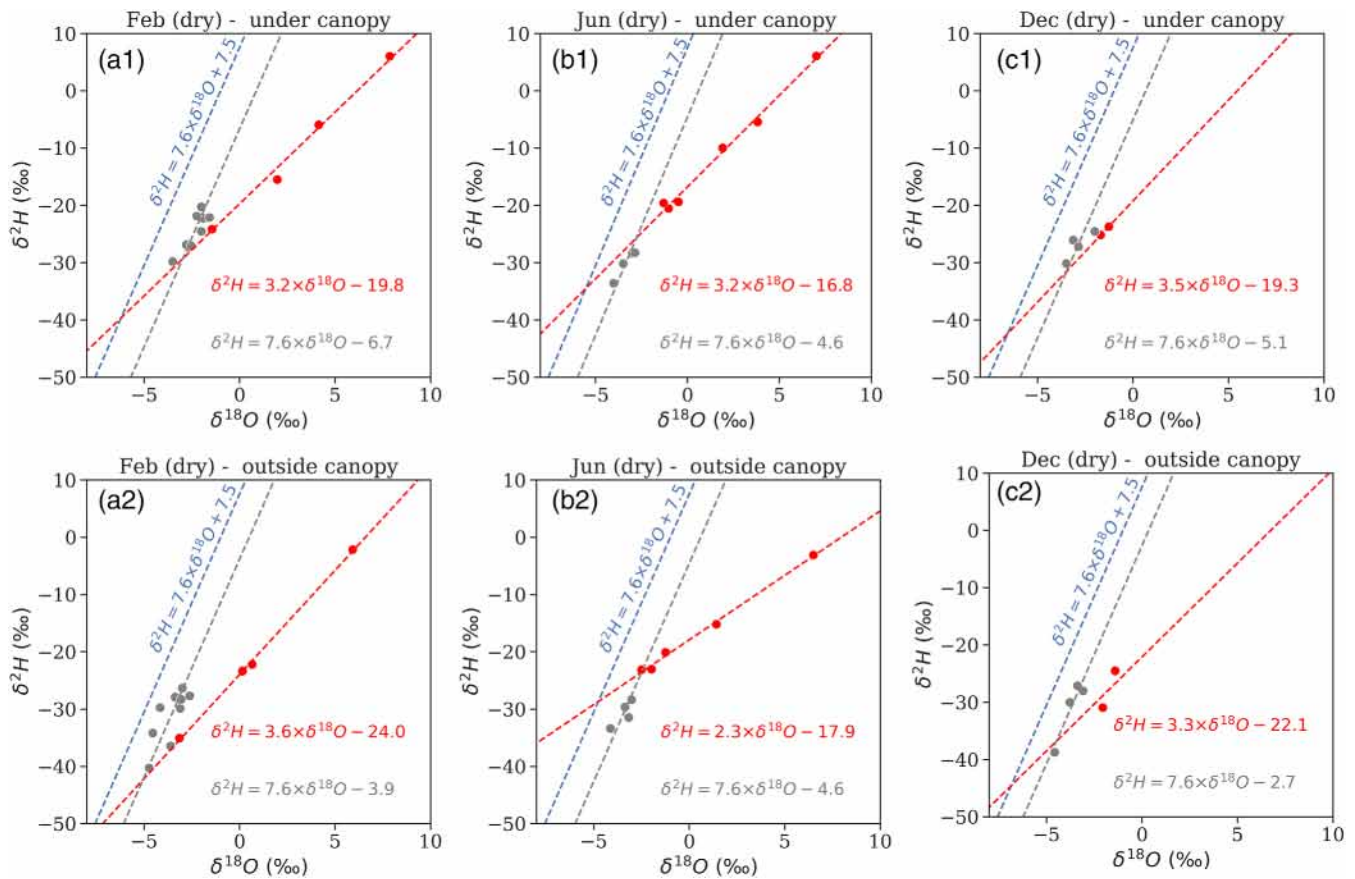


FIGURE 7 Relationship between $\delta^2\text{H}$ and $\delta^{18}\text{O}$ ratios in site 1 soil samples collected from the upper slope, under and outside tree canopies, during the months of February (a1, a2), June (b1, b2), and December (c1, c2). The blue dashed line is the LMWL. Red circles (with a red regression line) correspond to soil samples from the near-surface zone below the evaporation front. Grey circles and the dashed grey regression line correspond to soil samples from the zone below the evaporation front. Note that the grey regression line is parallel to the LMWL, but has an offset. (I.e., a different $\delta^2\text{H}$ intercept.)

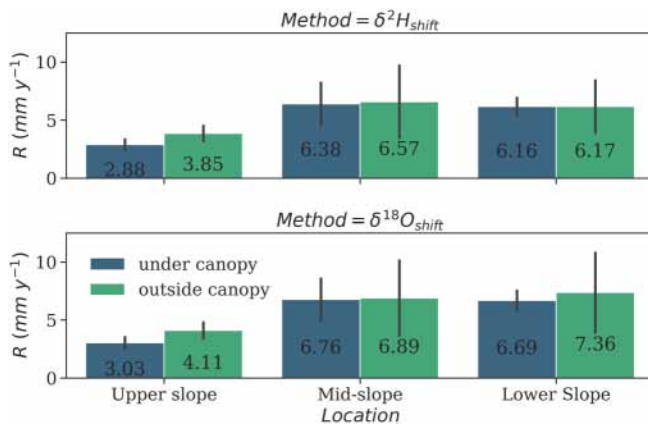


FIGURE 8 Mean annual groundwater recharge of the CT aquifer underneath and outside tree canopies at site 1, based upon analyses of the $\delta^2\text{H}_{\text{shift}}$ and $\delta^{18}\text{O}_{\text{shift}}$. Error bars show the standard deviation associated with each sampling period (February, June, and December).

distances from the coastline. The sites' LMWLs differ, too, from the LMWL that Travi et al. (1987) calculated for Senegal as a whole. We explore the differences below.

The LMWLs for Sites 1 and 2 are, respectively, $\delta^2\text{H} = 7.61 \pm 0.20 \times \delta^{18}\text{O} + 7.50 \pm 1.23$ ($R^2 = 0.98$), and $\delta^2\text{H} = 7.48 \pm 0.22 \times \delta^{18}\text{O} + 6.8 \pm 1.3$ ($R^2 = 0.98$). By comparison, the LMWL from Travi et al. (1987) ($\delta^2\text{H} = 7.93 \delta^{18}\text{O} + 10$ ($R^2 = 0.97$)) is closer to the GMWL ($\delta^2\text{H} = 8 \times \delta^{18}\text{O} + 10$, Craig (1961)), and was derived from a set of weighted monthly means of rainfall at seven different stations across Senegal during the 1981 monsoon. The monsoon vapour that condensed over Senegal during that time would have originated from the ocean; therefore, the average LMWL for the whole for the country (which is what Travi et al. estimated) would have been close to the GMWL.

As monsoon vapour moves inland, it becomes enriched in heavy isotopes due to evaporation. For that reason, the slopes and intercepts of the study sites' LMWLs are lower than those calculated by Travi et al. Moreover, the slope and intercept for Site 2 are lower than those of Site 1—as would be expected, because Site 2 is both farther from the coast and more arid: the annual rainfall is about 500 at Site 1, but only 300 mm at Site 2 (Figure 1). We note, too, that Travi et al. found that in the north of Senegal (at Richard Toll, close to Site 2), the heavy-isotope contents of rainfall increased with temperature, especially as the amount of rainfall decreased. However, no such “amount

effect" (i.e., relationship between rainfall amount and depletion in the heavy isotope) was evident in the present study.

4.2 | Stage II evaporation and the applicability of the isothermal-evaporation model

Evaporation from a bare soil surface proceeds in two fairly distinct stages (Fisher, 1923; Pearse et al., 1949). During Stage I (the "constant-rate" stage), evaporation occurs isothermally at a constant rate from a wet soil that meets the evaporative demand. As the soil surface begins to dry, the evaporation rate falls quickly at first, then enters Stage II (the "falling-rate" stage), during which the rate decreases gradually over time (Gardner, 1959). At both of our experimental sites, the evaporation process is probably in Stage II during the long dry season.

As applied to those sites, the bias in the isothermal model may be significant, primarily because of the uncertainty in the position of the evaporation front, which is the most critical input to the evaporation estimates (see Table 2). A relative standard deviation of about 25% was estimated by Allison and Barnes (1983) in their study. Although the uncertainty associated with the position of the evaporation front may be smaller in our study (because of the high vertical resolution of our sampling near the soil surface), other significant errors may have resulted from ignoring the vertical temperature gradient in the topsoil (Barnes et al., 1989). For example, the average soil temperature at 14:00 h at Site 1 during February fell from 39.8°C at the 2 cm depth to 30.4°C at 30 cm.

These caveats notwithstanding, we note that even allowing for the significant uncertainty in the E_a estimates, the estimated E_a at Site 1 amounts to only 4.7% of the total ET_a (which was based upon eddy covariance). The explanation for this low, unexpected E_a/ET_a ratio may be that most of the evaporation occurred during Stage I, when both the E_a and the T_a are high. This phenomenon was reported in the previous research on semi-arid sites, and which used the same approaches (e.g., Liu et al., 1995; Busari et al., 2013). Overall, the assumption of isothermal equilibrium evaporation seems to be valid. However, the model itself was developed for long-term evaporative losses, and therefore does not account for the first stage of evaporation, which is the most important one in semi-arid climatic conditions.

4.3 | Partitioning of E_a and T_a in groundnut fields and pasture

The calculated E_a and T_a rates for groundnut and pasture covers are reasonable, and within the range found in the literature for semi-arid regions under rainfed conditions (Chibarabada et al., 2020; Halilou et al., 2015; Kizito et al., 2012; Ratnakumar et al., 2009; Yopez et al., 2005). During the first evaluation period (the dry February–June months), the E_a fraction derived from the isotopic mass balance is low (0.02–0.06 mm d⁻¹) at both experimental sites, and on the same order of magnitude as values obtained from the steady-state isothermal

model. These low rates may be attributable to the low water contents and hydraulic conductivities of the sites' sandy soils during the dry season. However, we found that during the same period, E_a rates are much higher at the lower-slope locations in Site 2: 0.16 mm d⁻¹ according to the isothermal model, versus 0.12 mm d⁻¹ according to the isotope mass balance. These higher rates are probably due to the higher clay contents (and therefore greater water retention) in the topsoil at those locations.

During the second evaluation period (the dry-wet months June–August) and the last one (the wet-dry months August–December), the evaporation rates at both sites, as derived from the isotopic mass balance, are higher than during the first period. The difference is due to the increase in soil wetness in the wet season. These mass-balance evaporation rates are also higher than those obtained from the isothermal model (second-stage evaporation) for the same period. Therefore, the isotope mass balance captures both first- and second-stage evaporation from June to December. However, this method gave a negative E_a fraction (reported here as 0 mm d⁻¹) for the lower-slope location under the canopy cover (Site 1) during June–August. At the end of this period, the soil water at this location was more depleted in heavy isotopes ($\delta_f = -5.6$ ‰) than at the beginning ($\delta_i = -1.4$ ‰). It was also more depleted in heavy isotopes than the rainfall ($\delta_p = -4.9$ ‰). This discrepancy cannot be the result of evaporation or non-fractionating processes (transpiration or percolation). However, a possible explanation is that the rainfall that had recently infiltrated the shallow soil may have been more depleted in heavy isotopes than the bulk samples from the rain collector, which took time-integrative samples for the whole evaluation period. This idea is supported by data in the present study, from both sites, that show a high variability in the isotopic compositions of rainfall samples that had been collected during short time intervals. Similar variability is reported by other authors (e.g., Robertson & Gazis, 2006; Smith et al., 1979). In the present study, satisfactory ET_a partitioning values were obtained from time-integrative data (e.g., over the space of a season). However, more detailed information on the time dependence of partitioning could be obtained by sampling the soil more frequently (e.g., monthly, or weekly during the growing season) or via in-situ isotopic measurements of soil water (e.g., Gaj et al., 2016).

Regarding the reliability of the water-vapour equilibration method, it should be emphasized that to avoid fractionation effects, our samples were analysed as soon as possible after collection—a protocol that is challenging to implement when samples are taken in remote arid areas, and laboratories are far away. Still, it has been shown that even after being stored for several days in Ziploc bags of the specific type used in the present study, water samples do not fractionate to a degree that biases isotope analyses significantly (Hendry et al., 2015; Wassenaar et al., 2008). For longer storage, metallized bags might be used. However, gas build-up could bias the isotope analyses (Gralher et al., 2016, 2018). In the present study, water loss during sample preparation in the laboratory (see Section 2.3.2) was negligible (<0.15 ml, with no consistent deuterium-excess). In addition, by running mass balances on both $\delta^{18}\text{O}$ and $\delta^2\text{H}$, our isotope mass balance calculations may have accounted to some extent (at least

indirectly) for any fractionation processes that occurred during shipping or under laboratory conditions—which are different from those in the field. Finding the best storage container for shipping samples will require detailed studies.

4.4 | Comparison of groundnut ET_a partitioning to results from modelling approach

At Site 1, the ET_a that was calculated via the isotope approach is similar to the value that was obtained from eddy covariance (EC) measurements, except for the first evaluation period (the dry months February–June) (Table 3). The reason for that discrepancy may be that during the dry season, the water compositions that are used as inputs for the isotope approach reflect the second-stage evaporation from the soil, while the EC measurements may capture additional fluxes such as transpiration from shrubs and nearby trees. For mid-slope locations in open areas (outside tree canopies), the ET_a values obtained via validated HYDRUS-1D calculations (Diongue et al., 2022) are on the same order of magnitude as those from isotope mass balances and EC flux values. However, those methods do not predict the same partitioning of E_a and T_a for those locations, probably due to differences among the models' respective assumptions and partitioning approaches.

Specifically, the HYDRUS-1D model's procedure calculates the partitioning by reducing ET_0 to rates of T_a and E_a . The calculation of T_a is accomplished by applying (i) a surface-cover fraction that is based upon Beer's law (Ritchie, 1972), and (ii) a water-stress-reduction function (Feddes et al., 1978; Van Genuchten, 1987). To compute E_a , HYDRUS-1D uses a surface-pressure threshold (h_{critA}) and boundary conditions (Šimůnek et al., 2008). In contrast, the isotope approach is based upon measurements of isotope ratios (of precipitation and bulk soil water) at the beginning and end of a time interval. Those measurements are used as inputs to a simple mass balance, which assumes that deep percolation and transpired water are not affected by fractionation.

Overall, the isotope mass balance method gives higher values of T_a , while HYDRUS-1D gives higher values of E_a . Results from the isotope approach are more consistent with previous studies (e.g., Ferretti et al., 2003; Liebhard et al., 2022; Robertson & Gazis, 2006; Sutanto et al., 2012; Wang et al., 2010; Wenninger et al., 2010; Zhang et al., 2011). Those studies estimated the T_a/ET_a ratio at around 70%. In addition, the transpiration ratio obtained by the isotope approach is on the same order of magnitude as those reported by global studies

(e.g., Jasechko et al., 2013). In contrast the E_a/ET_a ratios that were calculated via HYDRUS-1D were around 76.8%. These differences suggest that to predict the partitionings of E_a and T_a accurately for sites such as ours, the HYDRUS-1D model may require further improvements (Kool et al., 2014). The improvements might include (i) optimizing the water-stress function (e.g., Feddes threshold) for groundnut crops (not yet performed, to our knowledge); and (ii) improving the above-mentioned ET_0 partitioning to potential evaporation and transpiration, which are currently based upon rough assumptions such as the surface-cover fraction and the Leaf Area Index (Beer's law).

4.5 | Soil water movement and groundwater recharge

Mechanisms of soil water movement can be identified by comparing the isotopic compositions of rainfall, soil water, and groundwater. During the dry season, the heavy-isotope enrichment of shallow soil water at both sites was higher than in the local rainfall. At the same time, a distinct evaporation front—the location of the most-negative lc -excess—was formed by fractionation in the upper soil zone. The shape of the isotope profiles in that zone varied as a function of depth during the wet season as rainfall infiltrated and mixed with the bulk soil water. (See the isotope profiles for the August sampling period in Figures 3 and 4.)

The $\delta^{18}O$ patterns in the deep soil zone, as well as the similarity between that zone's $\delta^{18}O$ values and those of groundwater, could be a result of deep soil water percolating down to the groundwater during the wet season. Other possible explanations include diffusion and equilibrium via a capillary rise. The latter possibility is supported by the deep soil's relatively constant water content: 0.103 – 0.119 cm^3 cm^{-3} , as measured by a Time Domain Reflectometer (TDR) sensor installed at a depth of 380 cm at the mid-slope location in Site 1 (supplementary materials, Figure S5b). One mechanism that would not have been detected via TDR sensors is groundwater recharge through preferential pathways—or perhaps by lateral flow. Those mechanisms might explain why the water table had risen about 50 cm by the end of the wet season (Figure S5c), and also why there was a nearly two-month delay between rainfall events and groundwater fluctuations.

The plausibility of preferential pathways and lateral flow at Site 1 is increased by reports that groundwater recharge of the CT aquifer in Sahel regions occurs mainly through “focused” mechanisms (e.g., Desconnets et al. 1997; Massuel et al. 2011, Favreau et al.

TABLE 3 Cumulative evapotranspiration (ET_a) and the partitioning between evaporation (E_a) and transpiration (T_a) at the mid-slope location outside the canopy at site 1 during the three evaluation periods, as determined via the isotope mass balance (imb), isothermal evaporation model (iem), and HYDRUS-1D numerical model (Hvd). All values are in mm.

Period	Location	E_a (iem)	E_a (imb)	E_a (Hvd)	T_a (imb)	T_a (Hvd)	ET_a (imb)	ET_a (Hvd)	ET_a (Ec)
Feb-Jun	Mid-slope	0.18	0.7	9.1	0.0	0.0	0.7	9.1	17.9
Jun-Aug	Mid-slope	0.11	23.9	104.3	58.2	8.5	82.1	112.8	94.8
Aug-Dec	Mid-slope	0.21	58.3	189.6	263.1	82.9	321.5	272.5	321.5

2009). Preferential flow allows water to bypass the soil matrix (Beven & Germann, 1982). As a result, young water can infiltrate deeply into the ground (Thomas et al., 2013), thereby contributing rapidly to groundwater replenishment rather than refilling the soil matrix. In this way, replenishment occurs with little exchange or mixing between young, mobile water and bulk soil water (Benettin et al., 2019; Evaristo et al., 2019; Sprenger et al., 2019; Stump & Maloszewski, 2010).

An example of this phenomenon is reported by Favreau et al. (2009), who showed that in Niger, at a site similar to our Site 1, recharge occurred via preferential flow through the edges of ponds or gullies—including at the outlets of gullies. Because these terrain features were the main recharge sites, aquifer-recharge rates rose tenfold over the space of 50 years as surface runoff increased in response to the clearing of natural savannah lands for rainfed crops. Specifically, the increase in lengths of gullies and surface areas of ponds (Leblanc et al. 2008) contributed to raising recharge rates from a few mm year⁻¹ in the 1950 s–1960 s to as much as 25 mm year⁻¹ in the 1990s–2000s (Favreau et al. 2009; Boucher et al. 2012).

The possibility of preferential pathways notwithstanding, our estimate that groundwater recharge amounts to <2% of annual rainfall (as calculated per the piston displacement method) is consistent with reported values from other semi-arid regions (e.g., Gaj et al., 2016; Koeniger et al., 2016; Skrzypek et al., 2019; Boumaiza et al., 2021; Edmunds and Gaye, 1994; Scanlon et al., 2006). In addition, our estimate of deep drainage below 2 m depth during the dry season, as calculated by the validated HYDRUS-1D, is similar to the groundwater recharges obtained via the piston-displacement method. The former values ranged from 1.7 mm during February–June to 5.0 mm during June–August. In contrast, the estimated deep drainage for the wet season was 68.3 mm. However, it should be recalled that although the piston-displacement method uses $\delta^2\text{H}_{\text{shift}}$ and $\delta^{18}\text{O}_{\text{shift}}$ values from a deeper soil layer (400–500 cm depth), and therefore takes into account the entire root zone (e.g., potential impact of shrubs and trees), this method fails to capture potential preferential pathways that may have caused the observed substantial fluctuation in groundwater levels.

5 | SUMMARY AND CONCLUSION

We characterized the stable isotopic compositions of rainfall, soil water, and groundwater at two sites along a climate gradient in Senegal (Site 1 in the Groundnut basin, and Site 2 in the Ferlo Valley). The slopes and intercepts of both sites' computed LMWLs were lower than those of the GMWL, reflecting isotopic fractionation. Isotopic analyses of bulk soil water revealed two distinct depth zones. The first was a zone of shallow soil water extending from the ground surface down to 150 cm at Site 1, and 100 cm at Site 2. Within this zone, isotope ratios of the soil water varied with depth and time due to evaporation and rainfall infiltration. In the second, deeper zone (150–500 cm at Site 1, and 100–300 cm at Site 2), the isotopic composition of the soil water was nearly constant.

During the dry season at both sites, a definite evaporation front was present in the shallow soil zone. This front, whose depth could be identified because it corresponded to the highest isotope ratios in the soil profile, allowed us to use the isothermal evaporation model to estimate second-stage evaporation rates. These ranged from 0.02–0.09 mm d⁻¹ at Site 1, and 0.02–0.11 mm d⁻¹ at Site 2.

In addition, we used mass balances of water and stable isotopes to partition E_a and T_a from the groundnut crop (Site 1) and pasture (Site 2) over three evaluation periods. During the first period (the dry months February–June), the soil was bare, with limited upward water fluxes due to low soil water contents and reduced soil hydraulic conductivity. E_a rates during this period were 0.03–0.06 and 0.02–0.16 mm d⁻¹ for Site 1 and Site 2, respectively. The second period (the dry-wet months June–August) marked the first stage of vegetation growth, when T_a is the main component of water loss. Rates for that component during the second period were 0.55–1.25 mm d⁻¹ for groundnut (Site 1), and 0.57–0.9 mm d⁻¹ for pasture (Site 2). During the third period—the wet (August) and dry (December) months, when crops mature and are harvested— T_a increased to 1.96–2.24 mm d⁻¹ for groundnut and 1.30–1.63 mm d⁻¹ for pasture.

In general, the isotope approach gave reasonable E_a and T_a rates for groundnut and pasture, and the partitioning ratios were within the range found in the literature. ET_a values from the isotope approach were similar to EC measurements, and also to values computed previously for Site 1 via a validated HYDRUS-1D model. However, the isotope mass balance gave a higher T_a/ET_a ratio (72%) than the HYDRUS-1D model (23.2%). Therefore, future research should include field measurements of E_a (e.g., using lysimeters or flux chamber methods) to further investigate the reliability of the isotope approach versus numerical modelling.

The average groundwater recharge of the CT aquifer, as estimated from the piston displacement method, was 5.44 ± 2.2 mm y⁻¹—less than 2% of Site 1's yearly rainfall. However, the magnitudes and timings of groundwater-level fluctuations suggest that to some degree, the CT aquifer was being recharged via preferential pathways. To infer and confirm the local regimes of soil-water movement, a comprehensive investigation should be performed, including the isotopic compositions of both the mobile water and the bulk soil water. In addition, piezometers should be installed along ponds and gullies to monitor groundwater levels.

ACKNOWLEDGEMENTS

D.M.L. Diongue received grants for the Ferlo experimental site from the Labex DRIIHM, and the French programme “Investissements d'Avenir” (ANR-11-LABX-0010), managed by the ANR. He also received funding from CIRAD/IRD/EDEQUE, and is grateful to all Sophy's members for their warm hospitality during his stay in Vienna. Faidherbia-Flux received funding from EU-LEAP-Agri (RAMSES II), EU-DESIRA (CASSECS), EU-H2020 (SustainSahel), AGROPOLIS, and TOTAL Foundations (DSCATT), CGIAR (GLDC). We are extremely grateful to the people of Sob-Niakhar and Widou Thingoly, particularly I. Diouf, A. Diouf, R. Diatte, M. Sy, B. Sow, and Sergent Badji. We also thank Dr. James Smith (<https://mx.linkedin.com/in/james-smith->

1b195047) who revised the English, and the two reviewers, whose observations greatly improved the paper.

DATA AVAILABILITY STATEMENT

The data that support the findings of this study are available for scientific purposes from the corresponding author upon request.

ORCID

Djim M. L. Diongue  <https://orcid.org/0000-0003-0905-9263>

Christine Stumpp  <https://orcid.org/0000-0001-9041-2735>

REFERENCES

- Adomako, D., Maloszewski, P., Stumpp, C., Osae, S., & Akiti, T. T. (2010). Estimating groundwater recharge from water isotope ($\delta^2\text{H}$, $\delta^{18}\text{O}$) depth profiles in the Densu River basin, Ghana. *Hydrological Sciences Journal*, 55, 1405–1416. <https://doi.org/10.1080/02626667.2010.527847>
- Allen, R. G., Pereira, L. S., Raes, D., & Smith, M. (1998). Crop evapotranspiration-guidelines for computing crop water requirements-FAO irrigation and drainage paper 56. Fao, Rome 300, D05109.
- Allison, G. B., & Barnes, C. J. (1983). Estimation of evaporation from non-vegetated surfaces using natural deuterium. *Nature*, 301, 143–145.
- Allison, G. B., & Barnes, C. J. (1985). Estimation of evaporation from the normally “dry” Lake Frome in South Australia. *Journal of Hydrology*, 78, 229–242.
- Allison, G. B., Barnes, C. J., Hughes, M. W., & Leaney, F. W. J. (1983). Effect of climate and vegetation on oxygen-18 and deuterium profiles in soils. *Isotope Hydrology*, 105–123.
- Allison, G. B., Gee, G. W., & Tyler, S. W. (1994). Vadose-zone techniques for estimating groundwater recharge in arid and semiarid regions. *Soil Science Society of America Journal*, 58, 6–14. <https://doi.org/10.2136/sssaj1994.03615995005800010002x>
- Allison, G. B., & Hughes, M. W. (1983). The use of natural tracers as indicators of soil-water movement in a temperate semi-arid region. *Journal of Hydrology*, 60, 157–173.
- Baldocchi, D. (2014). Measuring fluxes of trace gases and energy between ecosystems and the atmosphere—the state and future of the eddy covariance method. *Global Change Biology*, 20, 3600–3609.
- Barnes, C. J., & Allison, G. B. (1988). Tracing of water movement in the unsaturated zone using stable isotopes of hydrogen and oxygen. *Journal of Hydrology*, 100, 143–176. [https://doi.org/10.1016/0022-1694\(88\)90184-9](https://doi.org/10.1016/0022-1694(88)90184-9)
- Barnes, C. J., Allison, G. B., & Hughes, M. W. (1989). Temperature gradient effects on stable isotope and chloride profiles in dry soils. *Journal of Hydrology*, 112, 69–87.
- Benettin, P., Queloz, P., Bensimon, M., McDonnell, J. J., & Rinaldo, A. (2019). Velocities, residence times, tracer breakthroughs in a vegetated lysimeter: A multitracer experiment. *Water Resources Research*, 55, 21–33.
- Benettin, P., Volkmann, T. H. M., von Freyberg, J., Frentress, J., Penna, D., Dawson, T. E., & Kirchner, J. W. (2018). Effects of climatic seasonality on the isotopic composition of evaporating soil waters. *Hydrology and Earth System Sciences*, 22, 2881–2890. <https://doi.org/10.5194/hess-22-2881-2018>
- Beven, K., & Germann, P. (1982). Macropores and water flow in soils. *Water Resources Research*, 18, 1311–1325.
- Beyer, M., Gaj, M., Hamutoko, J. T., Koeniger, P., Wanke, H., & Himmelsbach, T. (2015). Estimation of groundwater recharge via deuterium labelling in the semi-arid Cuvelai-Etosha Basin, Namibia. *Isotopes in Environmental and Health Studies*, 51, 533–552.
- Black, C. A. (1965). Method of soil analysis part 2. *Chemical and Microbiological Properties*, 9, 1387–1388.
- Blott, S. J., & Pye, K. (2001). GRADISTAT: A grain size distribution and statistics package for the analysis of unconsolidated sediments. *Earth Surface Processes and Landforms*, 26(11), 1237–1248.
- Boucher, M., Favreau, G., Nazoumou, Y., Cappelaere, B., Massuel, S., & Legchenko, A. (2012). Constraining groundwater modeling with magnetic resonance soundings. *Groundwater*, 50(5), 775–784.
- Boumaiza, L., Chesnaux, R., Drias, T., Walter, J., & Stumpp, C. (2021). Using vadose-zone water stable isotope profiles for assessing groundwater recharge under different climatic conditions. *Hydrological Sciences Journal*, 66, 1597–1609. <https://doi.org/10.1080/02626667.2021.1957479>
- Braud, I. (2002). *SiSPAT user's manual update*. Laboratoire d'Etude des Transferts en Hydrologie et Environnement.
- Busari, M. A., Salako, F. K., Tuniz, C., Zuppi, G. M., Stenni, B., Adetunji, M. T., & Arowolo, T. A. (2013). Estimation of soil water evaporative loss after tillage operation using the stable isotope technique. *International Agrophysics*, 27(3), 257–264. <https://doi.org/10.2478/v10247-012-0093-8>
- Caldwell, M. M., Dawson, T. E., & Richards, J. H. (1998). Hydraulic lift: Consequences of water efflux from the roots of plants. *Oecologia*, 113, 151–161.
- Chen, Y., Zhang, Z., Wang, X., Sun, S., Zhang, Y., Wang, S., Yang, M., Ji, F., Ji, C., & Xiang, D. (2022). Sap velocity, transpiration and water use efficiency of drip-irrigated cotton in response to chemical topping and row spacing. *Agricultural Water Management*, 267, 107611.
- Chibarabada, T. P., Modi, A. T., & Mabhaudhi, T. (2020). Calibration and evaluation of aquacrop for groundnut (*Arachis hypogaea*) under water deficit conditions. *Agricultural and Forest Meteorology*, 281, 107850.
- Christmann, D., & Sonntag, C. (1987). Groundwater evaporation from east-Saharan depressions by means of deuterium and oxygen-18 in soil moisture. In *Isotope techniques in water resources development*. AIEA.
- Clark, I. D., & Fritz, P. (1997). *Environmental isotopes in hydrogeology*. CRC Press.
- Conrad, G., & Lappartient, J.-R. (1987). Le ‘continental terminal’, sa place dans l'évolution géodynamique du bassin sénégal-Mauritanien durant le Cénozoïque. *Journal of African Earth Sciences*, 1983(6), 45–60.
- Craig, H. (1961). Standard for reporting concentrations of deuterium and oxygen-18 in natural waters. *Science*, 133, 1833–1834.
- Dawson, T. E. (1993). Hydraulic lift and water use by plants: Implications for water balance, performance and plant-plant interactions. *Oecologia*, 95, 565–574.
- Dawson, T. E., & Ehleringer, J. R. (1991). Streamside trees that do not use stream water. *Nature*, 350, 335–337.
- Dawson, T. E., & Ehleringer, J. R. (1998). Plants, isotopes and water use: A catchment-scale perspective. In *Isotope tracers in catchment hydrology* (pp. 165–202). Elsevier.
- Desconnets, J. C., Taupin, J. D., Lebel, T., & Leduc, C. (1997). Hydrology of the HAPEX-Sahel central super-site: Surface water drainage and aquifer recharge through the pool systems. *Journal of Hydrology*, 188–189, 155–178. [https://doi.org/10.1016/S0022-1694\(96\)03158-7](https://doi.org/10.1016/S0022-1694(96)03158-7)
- Diagne. (2014). *Groundnut marketing in Senegal: Issues, constraints and prospects: A study in the groundnut basin* (Msc thesis). Cheikh anta Diop University.
- Dincer, T., Al-Mugrin, A., & Zimmermann, U. (1974). Study of the infiltration and recharge through the sand dunes in arid zones with special reference to the stable isotopes and thermonuclear tritium. *Journal of Hydrology*, 23, 79–109.
- Diongue, D. M. L., Rouspard, O., Do, F. C., Stumpp, C., Orange, D., Sow, S., Jourdan, C., & Faye, S. (2022). Evaluation of parameterisation approaches for estimating soil hydraulic parameters with HYDRUS-1D in the groundnut basin of Senegal. *Hydrological Sciences Journal*, 67, 2327–2343. <https://doi.org/10.1080/02626667.2022.2142474>
- Do, F. C., Rocheteau, A., Diagne, A. L., Goudiaby, V., Granier, A., & Lhomme, J.-P. (2008). Stable annual pattern of water use by *Acacia*

- tortilis in Sahelian Africa. *Tree Physiology*, 28, 95–104. <https://doi.org/10.1093/treephys/28.1.95>
- Dongmann, G., Nürnberg, H. W., Förstel, H., & Wagener, K. (1974). On the enrichment of H_2^{18}O in the leaves of transpiring plants. *Radiation and Environmental Biophysics*, 11(1), 41–52.
- Dubbart, M., Cuntz, M., Piayda, A., Maguás, C., & Werner, C. (2013). Partitioning evapotranspiration – testing the Craig and Gordon model with field measurements of oxygen isotope ratios of evaporative fluxes. *Journal of Hydrology*, 496, 142–153. <https://doi.org/10.1016/j.jhydrol.2013.05.033>
- Evaristo, J., Kim, M., van Haren, J., Pangle, L. A., Harman, C. J., Troch, P. A., & McDonnell, J. J. (2019). Characterizing the fluxes and age distribution of soil water, plant water, and deep percolation in a model tropical ecosystem. *Water Resources Research*, 55, 3307–3327.
- Favreau, G., Cappelaere, B., Massuel, S., Leblanc, M., Boucher, M., Boulain, N., & Leduc, C. (2009). Land clearing, climate variability, and water resources increase in semiarid southwest Niger: A review. *Water Resources Research*, 45(7).
- Faye, B., & Du, G. (2021). Agricultural land transition in the “Groundnut Basin” of Senegal: 2009 to 2018. *Land*, 10, 996. <https://doi.org/10.3390/land10100996>
- Faye, N., Diallo, A., Sagna, M. B., Peiry, J. L., Sarr, P. S., & Guisse, A. (2022). Influence of anthropic and eco-hydrological factors on the floristic diversity of the herbaceous vegetation around the temporary ponds in Ferlo, northern Senegal. *Journal of Plant Ecology*, 15, 26–38. <https://doi.org/10.1093/jpe/rtab053>
- Faye, N., Diallo, M. D., Peiry, J. L., Diallo, A., & Guisse, A. (2020). Influence of anthropic and topographic factors on the physicochemical properties of the soil around temporary pools in Ferlo, North Senegal. *International Journal of Plant & Soil Science*, 32, 26–40.
- Faye, S. C., Diongue, M. L., Pouye, A., Gaye, C. B., Travi, Y., Wohnlich, S., Faye, S., & Taylor, R. G. (2019). Tracing natural groundwater recharge to the Thiarye aquifer of Dakar, Senegal. *Hydrogeology Journal*, 27, 1067–1080. <https://doi.org/10.1007/s10040-018-01923-8>
- Faye, W., Fall, A. N., Orange, D., Do, F., Roupsard, O., & Kane, A. (2020). Climatic variability in the sine-Saloum basin and its impacts on water resources: Case of the sob and Dioline watersheds in the region of Niakhar. *Proceedings of the International Association of Hydrological Sciences*, 383, 391–399.
- Feddes, R. A., Kowalik, P. J., & Zaradny, H. (1978). Simulation of field water use and crop yield. Simulation monographs. Pudoc, Wageningen 9-30.
- Ferretti, D. F., Pendall, E., Morgan, J. A., Nelson, J. A., Lecain, D., & Mosier, A. R. (2003). Partitioning evapotranspiration fluxes from a Colorado grassland using stable isotopes: Seasonal variations and ecosystem implications of elevated atmospheric CO_2 . *Plant and Soil*, 254, 291–303.
- Fisher, E. A. (1923). Some factors affecting the evaporation of water from soil. *The Journal of Agricultural Science*, 13, 121–143.
- Gaj, M., Beyer, M., Koeniger, P., Wanke, H., Hamutoko, J., & Himmelsbach, T. (2016). In situ unsaturated zone water stable isotope (2H and 18O) measurements in semi-arid environments: A soil water balance. *Hydrology and Earth System Sciences*, 20, 715–731. <https://doi.org/10.5194/hess-20-715-2016>
- Gardner, W. H. (1965). Water content. Methods of soil analysis: Part 1 physical and mineralogical properties. *Including Statistics of Measurement and Sampling*, 9, 82–127.
- Gardner, W. R. (1959). Solutions of the flow equation for the drying of soils and other porous media. *Soil Science Society of America Journal*, 23, 183–187.
- Gat, J. R. (1996). Oxygen and hydrogen isotopes in the hydrologic cycle. *Annual Review of Earth and Planetary Sciences*, 24, 225–262.
- Gaye, C. B., & Edmunds, W. M. (1996). Groundwater recharge estimation using chloride, stable isotopes and tritium profiles in the sands of northwestern Senegal. *Environmental Geology*, 27, 246–251.
- Glendening, G. E. (1941). Development of seedlings of *Heteropogon contortus* as related to soil moisture and competition. *Botanical Gazette*, 102, 684–698.
- Gong, C., Wang, W., Zhang, Z., Wang, H., Luo, J., & Brunner, P. (2020). Comparison of field methods for estimating evaporation from bare soil using lysimeters in a semi-arid area. *Journal of Hydrology*, 590, 125334. <https://doi.org/10.1016/j.jhydrol.2020.125334>
- Gralher, B., Herbstritt, B., Weiler, M., Wassenaar, L. I., & Stumpp, C. (2016). Correcting laser-based water stable isotope readings biased by carrier gas changes. *Environmental Science & Technology*, 50, 7074–7081. <https://doi.org/10.1021/acs.est.6b01124>
- Gralher, B., Herbstritt, B., Weiler, M., Wassenaar, L. I., & Stumpp, C. (2018). Correcting for biogenic gas matrix effects on laser-based pore water-vapor stable isotope measurements. *Vadose Zone Journal*, 17, 1–10. <https://doi.org/10.2136/vzj2017.08.0157>
- Granier, A. (1985). A new method of sap flow measurement in tree stems. In *Annales des Sciences Forestières* (Vol. 42, pp. 193–200).
- Grouzis, M., Diouf, M., Rocheteau, A., & Berger, A. (1998). Fonctionnement hydrique et réponses des ligneux sahéliens à l'aridité. In C. Campa, C. Grignon, M. Gueye (Eds.), *L'acacia au Sénégal*. (pp. 47–61). Paris: ORSTOM. (Colloques et Séminaires).
- Halilou, O., Hamidou, F., Taya, B. K., Mahamane, S., & Vadez, V. (2015). Water use, transpiration efficiency and yield in cowpea (*Vigna unguiculata*) and peanut (*Arachis hypogaea*) across water regimes. *Crop & Pasture Science*, 66, 715. <https://doi.org/10.1071/CP14182>
- Hendry, M. J., Schmeling, E., Wassenaar, L. I., Barbour, S. L., & Pratt, D. (2015). Determining the stable isotope composition of pore water from saturated and unsaturated zone core: Improvements to the direct vapour equilibration laser spectrometry method. *Hydrology and Earth System Sciences*, 19, 4427–4440. <https://doi.org/10.5194/hess-19-4427-2015>
- Herczeg, A. L., & Leaney, F. W. (2011). Environmental tracers in arid-zone hydrology. *Hydrogeology Journal*, 19, 17–29.
- Horita, J., Rozanski, K., & Cohen, S. (2008). Isotope effects in the evaporation of water: A status report of the Craig-Gordon model. *Isotopes in Environmental and Health Studies*, 44, 23–49.
- Horita, J., & Wesolowski, D. J. (1994). Liquid-vapor fractionation of oxygen and hydrogen isotopes of water from the freezing to the critical temperature. *Geochimica et Cosmochimica Acta*, 58, 3425–3437.
- Jasechko, S., Sharp, Z. D., Gibson, J. J., Birks, S. J., Yi, Y., & Fawcett, P. J. (2013). Terrestrial water fluxes dominated by transpiration. *Nature*, 496, 347–350. <https://doi.org/10.1038/nature11983>
- Kelliher, F. M., Köstner, B. M. M., Hollinger, D. Y., Byers, J. N., Hunt, J. E., McSeveny, T. M., Meserth, R., Weir, P. L., & Schulze, E.-D. (1992). Evaporation, xylem sap flow, and tree transpiration in a New Zealand broad-leaved forest. *Agricultural and Forest Meteorology*, 62, 53–73.
- Kizito, F., Dragila, M. I., Senè, M., Brooks, J. R., Meinzer, F. C., Diedhiou, I., Diouf, M., Lufafa, A., Dick, R. P., & Selker, J. (2012). Hydraulic redistribution by two semi-arid shrub species: Implications for Sahelian agroecosystems. *Journal of Arid Environments*, 83, 69–77.
- Koeniger, P., Gaj, M., Beyer, M., & Himmelsbach, T. (2016). Review on soil water isotope-based groundwater recharge estimations: Review soil water isotope. *Hydrological Processes*, 30, 2817–2834. <https://doi.org/10.1002/hyp.10775>
- Kool, D., Agam, N., Lazarovitch, N., Heitman, J. L., Sauer, T. J., & Ben-Gal, A. (2014). A review of approaches for evapotranspiration partitioning. *Agricultural and Forest Meteorology*, 184, 56–70.
- Landwehr, J. M., Coplen, T. B., 2006. Line-conditioned excess: A new method for characterizing stable hydrogen and oxygen isotope ratios in hydrologic systems, in: International conference on isotopes in environmental studies. IAEA Vienna, pp. 132–135.
- Leblanc, M. J., Favreau, G., Massuel, S., Tweed, S. O., Loireau, M., & Cappelaere, B. (2008). Land clearance and hydrological change in the Sahel: SW Niger. *Global and Planetary Change*, 61(3–4), 135–150. <https://doi.org/10.1016/j.gloplacha.2007.08.011>

- Liebhards, G., Klik, A., Stumpp, C., & Nolz, R. (2022). Partitioning evapotranspiration using water stable isotopes and information from lysimeter experiments. *Hydrological Sciences Journal*, 67, 646–661. <https://doi.org/10.1080/02626667.2022.2030866>
- Liu, B., Phillips, F., Hoines, S., Campbell, A. R., & Sharma, P. (1995). Water movement in desert soil traced by hydrogen and oxygen isotopes, chloride, and chlorine-36, southern Arizona. *Journal of Hydrology*, 168 (1–4), 91–110.
- Liu, M., Shi, H., Paredes, P., Ramos, T. B., Dai, L., Feng, Z., & Pereira, L. S. (2022). Estimating and partitioning maize evapotranspiration as affected by salinity using weighing lysimeters and the SIMDualKc model. *Agricultural Water Management*, 261, 107362. <https://doi.org/10.1016/j.agwat.2021.107362>
- Lu, X., Liang, L. L., Wang, L., Jenerette, G. D., McCabe, M. F., & Grantz, D. A. (2017). Partitioning of evapotranspiration using a stable isotope technique in an arid and high temperature agricultural production system. *Agricultural Water Management*, 179, 103–109.
- Maignien, R. (1965). Notice explicative: carte pédologique du Sénégal au 1/1.000.000.
- Marrero, T. R., & Mason, E. A. (1972). Gaseous diffusion coefficients. *Journal of Physical and Chemical Reference Data*, 1(1), 3–118.
- Massuel, S., Cappelaere, B., Favreau, G., Leduc, C., Lebel, T., & Vischel, T. (2011). Integrated surface water–groundwater modelling in the context of increasing water reserves of a regional Sahelian aquifer. *Hydrological Sciences Journal*, 56(7), 1242–1264.
- Merlivat, L. (1978). Molecular diffusivities of H 2 16 O, HD 16 O, and H 2 18 O in gases. *The Journal of Chemical Physics*, 69, 2864–2871.
- Moriana, A., Orgaz, F., Pastor, M., & Fereres, E. (2003). Yield responses of a mature olive orchard to water deficits. *Journal of the American Society for Horticultural Science*, 128, 425–431. <https://doi.org/10.21273/JASHS.128.3.0425>
- Mueller, M. H., Alaoui, A., Kuells, C., Leistert, H., Meusburger, K., Stumpp, C., Weiler, M., & Alewell, C. (2014). Tracking water pathways in steep hillslopes by $\delta^{18}\text{O}$ depth profiles of soil water. *Journal of Hydrology*, 519, 340–352.
- Ndiaye, O., Diop, A. T., Diène, M., & Akpo, L. E. (2015). Étude comparée de la végétation de 1964 et 2011 en milieu pâturé: Cas du CRZ de Dahra. *Journal of Applied Biosciences*, 88, 8235–8248.
- Niang, K. (2009). *The tree in the community rangelands of Ferlo-Nord (Senegal)* (Master Thesis). Université Cheikh Anta Diop.
- Nielsen, D. C., & Vigil, M. F. (2010). Precipitation storage efficiency during fallow in wheat-fallow systems. *Agronomy Journal*, 102, 537–543.
- Niemi, J., Hyttiäinen, K., Camara, A., Fall, C., & Msangi, S. (Eds.). (2015). A dynamic model to analyze the sustainability of extensive common-pasture-based livestock husbandry in Sahel. <https://doi.org/10.22004/ag.econ.212531>
- Nouri, H., Beecham, S., Kazemi, F., & Hassanli, A. M. (2013). A review of ET measurement techniques for estimating the water requirements of urban landscape vegetation. *Urban Water Journal*, 10, 247–259.
- Oerter, E., Slessarev, E., Visser, A., Min, K., Kan, M., McFarlane, K. J., Saha, M. C., Berhe, A. A., Pett-Ridge, J., & Nuccio, E. (2021). Hydraulic redistribution by deeply rooted grasses and its ecohydrologic implications in the southern Great Plains of North America. *Hydrological Processes*, 35, e14366.
- Pearse, J., Oliver, T., & Newitt, D. (1949). The mechanism of the drying of solids: Part I. the forces giving rise to movement of water in granular beds during drying. *Transactions. Institute of Chemical Engineers*, 27, 1–8.
- Penman, H. L. (1940). Gas and vapour movements in the soil: I. the diffusion of vapours through porous solids. *The Journal of Agricultural Science*, 30, 437–462.
- Pörtner, H.-O., Roberts, D.C., Tignor, M.M.B., Poloczanska, E.S., Mintenbeck, K., Alegría, A., Craig, M., Langsdorf, S., Löschke, S., Möller, V., Okem, A., Rama, B. (Eds.). 2022. *Climate change 2022: Impacts, adaptation and vulnerability*. Contribution of Working Group II to the Sixth Assessment Report of the Intergovernmental Panel on Climate Change. Cambridge University Press.
- Priyadarshini, K. V. R., Prins, H. H., de Bie, S., Heitkönig, I. M., Woodborne, S., Gort, G., Kirkman, K., Ludwig, F., Dawson, T. E., & de Kroon, H. (2016). Seasonality of hydraulic redistribution by trees to grasses and changes in their water-source use that change tree–grass interactions. *Ecohydrology*, 9, 218–228.
- Ratnakumar, P., Vadez, V., Nigam, S. N., & Krishnamurthy, L. (2009). Assessment of transpiration efficiency in peanut (*Arachis hypogaea* L.) under drought using a lysimetric system. *Plant Biology*, 11, 124–130.
- Raz-Yaseef, N., Rotenberg, E., & Yakir, D. (2010). Effects of spatial variations in soil evaporation caused by tree shading on water flux partitioning in a semi-arid pine forest. *Agricultural and Forest Meteorology*, 150, 454–462.
- Ritchie, J. T. (1972). Model for predicting evaporation from a row crop with incomplete cover. *Water Resources Research*, 8, 1204–1213.
- Robertson, J. A., & Gazis, C. A. (2006). An oxygen isotope study of seasonal trends in soil water fluxes at two sites along a climate gradient in Washington state (USA). *Journal of Hydrology*, 328, 375–387. <https://doi.org/10.1016/j.jhydrol.2005.12.031>
- Rothfuss, Y., Quade, M., Brüggemann, N., Graf, A., Vereecken, H., & Dubbert, M. (2021). Reviews and syntheses: Gaining insights into evapotranspiration partitioning with novel isotopic monitoring methods. *Biogeosciences*, 18, 3701–3732. <https://doi.org/10.5194/bg-18-3701-2021>
- Roupsard, O., Audebert, A., Ndour, A. P., Clermont-Dauphin, C., Agbohessou, Y., Sanou, J., Koala, J., Faye, E., Sambakhe, D., & Jourdan, C. (2020). How far does the tree affect the crop in agroforestry? New spatial analysis methods in a *Faidherbia* parkland. *Agriculture, Ecosystems & Environment*, 296, 106928.
- Roupsard, O., Bonnefond, J.-M., Irvine, M., Berbigier, P., Nouvellon, Y., Dauzat, J., Taga, S., Hamel, O., Jourdan, C., & Saint-André, L. (2006). Partitioning energy and evapo-transpiration above and below a tropical palm canopy. *Agricultural and Forest Meteorology*, 139, 252–268.
- Scanlon, B. R., Healy, R. W., & Cook, P. G. (2002). Choosing appropriate techniques for quantifying groundwater recharge. *Hydrogeology Journal*, 10, 18–39.
- Scanlon, B. R., Keese, K. E., Flint, A. L., Flint, L. E., Gaye, C. B., Edmunds, W. M., & Simmers, I. (2006). Global synthesis of groundwater recharge in semiarid and arid regions. *Hydrological Processes*, 20, 3335–3370. <https://doi.org/10.1002/hyp.6335>
- Selaolo, E. T., Beekman, H. E., Gieske, A. S. M., & De Vries, J. J. (2003). *Multiple tracer profiling in GRES findings*.
- Shuttleworth, W. J., & Wallace, J. S. (1985). Evaporation from sparse crops—an energy combination theory. *Quarterly Journal of the Royal Meteorological Society*, 111(469), 839–855.
- Sieglwart, L., Bertrand, I., Roupsard, O., Duthoit, M., & Jourdan, C. (2022). Root litter decomposition in a sub-Saharan agroforestry parkland dominated by *Faidherbia albida*. *Journal of Arid Environments*, 198, 104696.
- Sileshi, G. W. (2016). The magnitude and spatial extent of influence of *Faidherbia albida* trees on soil properties and primary productivity in drylands. *Journal of Arid Environments*, 132, 1–14.
- Šimůnek, J., Šejna, M., Saito, H., Sakai, M., & Van Genuchten, M. T. (2008). The HYDRUS-1D software package for simulating the movement of water, heat, and multiple solutes in variably saturated media, version 4.0. *HYDRUS software series*, 3, 315.
- Skrzypek, G., Dogramaci, S., Page, G. F. M., Rouillard, A., & Grierson, P. F. (2019). Unique stable isotope signatures of large cyclonic events as a tracer of soil moisture dynamics in the semiarid subtropics. *Journal of Hydrology*, 578, 124124. <https://doi.org/10.1016/j.jhydrol.2019.124124>
- Skrzypek, G., Mydlowski, A., Dogramaci, S., Hedley, P., Gibson, J. J., & Grierson, P. F. (2015). Estimation of evaporative loss based on the stable isotope composition of water using Hydrocalculator. *Journal of Hydrology*, 523, 781–789.

- Smith, G. I., Friedman, I., Klieforth, H., & Hardcastle, K. (1979). Areal distribution of deuterium in eastern California precipitation, 1968–1969. *Journal of Applied Meteorology and Climatology*, 18, 172–188.
- Sprenger, M., Stumpp, C., Weiler, M., Aeschbach, W., Allen, S. T., Benettin, P., Dubbert, M., Hartmann, A., Hrachowitz, M., Kirchner, J. W., McDonnell, J. J., Orlowski, N., Penna, D., Pfahl, S., Rinderer, M., Rodriguez, N., Schmidt, M., & Werner, C. (2019). The demographics of water: A review of water ages in the critical zone. *Reviews of Geophysics*, 57, 800–834. <https://doi.org/10.1029/2018RG000633>
- Sprenger, M., Tetzlaff, D., & Soulsby, C. (2017). Soil water stable isotopes reveal evaporation dynamics at the soil–plant–atmosphere interface of the critical zone. *Hydrology and Earth System Sciences*, 21, 3839–3858. <https://doi.org/10.5194/hess-21-3839-2017>
- Stumpp, C., & Kammerer, G. (2022). The Vadose zone—A semi-aquatic ecosystem. In T. Mehner & K. Tockner (Eds.), *Encyclopedia of inland waters* (Second ed., pp. 331–338). Oxford: Elsevier. <https://doi.org/10.1016/B978-0-12-819166-8.00179-1>
- Stumpp, C., & Maloszewski, P. (2010). Quantification of preferential flow and flow heterogeneities in an unsaturated soil planted with different crops using the environmental isotope $\delta^{18}\text{O}$. *Journal of Hydrology*, 394, 407–415.
- Sutanto, S. J., Wenninger, J., Coenders-Gerrits, A. M. J., & Uhlenbrook, S. (2012). Partitioning of evaporation into transpiration, soil evaporation and interception: A comparison between isotope measurements and a HYDRUS-1D model. *Hydrology and Earth System Sciences*, 16, 2605–2616. <https://doi.org/10.5194/hess-16-2605-2012>
- Tappan, G. G., Sall, M., Wood, E. C., & Cushing, M. (2004). Ecoregions and land cover trends in Senegal. *Journal of Arid Environments*, 59, 427–462.
- Thomas, E. M., Lin, H., Duffy, C. J., Sullivan, P. L., Holmes, G. H., Brantley, S. L., & Jin, L. (2013). Spatiotemporal patterns of water stable isotope compositions at the Shale Hills critical zone observatory: Linkages to subsurface hydrologic processes. *Vadose Zone Journal*, 12, 1–16.
- Travi, Y., Gac, J.-Y., Fontes, J. C., & Fritz, B. (1987). Reconnaissance chimique et isotopique des eaux de pluie au Sénégal. *Géodynamique*, 2, 43–53.
- van Dam, J. C., Groenendijk, P., Hendriks, R. F., & Kroes, J. G. (2008). Advances of modeling water flow in variably saturated soils with SWAP. *Vadose Zone Journal*, 7, 640–653.
- Van Genuchten, M. T. (1987). *A numerical model for water and solute movement in and below the root zone*. United States Department of Agriculture Agricultural Research Service US.
- Vincke, C., Diédhiou, I., & Grouzis, M. (2010). Long term dynamics and structure of woody vegetation in the Ferlo (Senegal). *Journal of Arid Environments*, 74, 268–276.
- Wang, L., Caylor, K. K., Villegas, J. C., Barron-Gafford, G. A., Breshears, D. D., & Huxman, T. E. (2010). Partitioning evapotranspiration across gradients of woody plant cover: Assessment of a stable isotope technique. *Geophysical Research Letters*, 37, L09401. <https://doi.org/10.1029/2010GL043228>
- Wang, L., Good, S. P., Caylor, K. K., & Cernusak, L. A. (2012). Direct quantification of leaf transpiration isotopic composition. *Agricultural and Forest Meteorology*, 154, 127–135.
- Wassenaar, L. I., Hendry, M. J., Chostner, V. L., & Lis, G. P. (2008). High resolution pore water $\delta^2\text{H}$ and $\delta^{18}\text{O}$ measurements by H_2O (liquid)- H_2O (vapor) equilibration laser spectroscopy. *Environmental Science & Technology*, 42, 9262–9267.
- Wenninger, J., Beza, D. T., & Uhlenbrook, S. (2010). Experimental investigations of water fluxes within the soil–vegetation–atmosphere system: Stable isotope mass-balance approach to partition evaporation and transpiration. *Physics and Chemistry of the Earth, Parts A/B/C*, 35, 565–570. <https://doi.org/10.1016/j.pce.2010.07.016>
- Windhorst, D., Kraft, P., Timbe, E., Frede, H.-G., & Breuer, L. (2014). Stable water isotope tracing through hydrological models for disentangling runoff generation processes at the hillslope scale. *Hydrology and Earth System Sciences*, 18, 4113–4127.
- Xu, J., Guo, Z., Li, Z., Li, F., Xue, X., Wu, X., Zhang, X., Li, H., Zhang, X., & Han, Q. (2021). Stable oxygen isotope analysis of the water uptake mechanism via the roots in spring maize under the ridge–furrow rain-water harvesting system in a semi-arid region. *Agricultural Water Management*, 252, 106879.
- Yang, Q., Xiao, H., Zhao, L., Zhou, M., Li, C., & Cao, S. (2010). Stable isotope techniques in plant water sources: A review. *Sciences in Cold and Arid Regions*, 2, 112–122.
- Yepez, E. A., Huxman, T. E., Ignace, D. D., English, N. B., Weltzin, J. F., Castellanos, A. E., & Williams, D. G. (2005). Dynamics of transpiration and evaporation following a moisture pulse in semiarid grassland: A chamber-based isotope method for partitioning flux components. *Agricultural and Forest Meteorology*, 132, 359–376. <https://doi.org/10.1016/j.agrformet.2005.09.006>
- Zahn, E., Bou-Zeid, E., Good, S. P., Katul, G. G., Thomas, C. K., Ghannam, K., Smith, J. A., Chamecki, M., Dias, N. L., & Fuentes, J. D. (2022). Direct partitioning of eddy-covariance water and carbon dioxide fluxes into ground and plant components. *Agricultural and Forest Meteorology*, 315, 108790.
- Zhang, Y., Shen, Y., Sun, H., & Gates, J. B. (2011). Evapotranspiration and its partitioning in an irrigated winter wheat field: A combined isotopic and micrometeorologic approach. *Journal of Hydrology*, 408, 203–211.
- Zimmermann, U., Münnich, K. O., & Roether, W. (1967). Downward movement of soil moisture traced by means of hydrogen isotopes. *Isotope techniques in the hydrologic cycle*, 11, 28–36.

SUPPORTING INFORMATION

Additional supporting information can be found online in the Supporting Information section at the end of this article.

How to cite this article: Diongue, D. M. L., Stumpp, C., Rouspard, O., Orange, D., Do, F. C., & Faye, S. (2023). Estimating water fluxes in the critical zone using water stable isotope approaches in the Groundnut and Ferlo basins of Senegal. *Hydrological Processes*, 37(1), e14787. <https://doi.org/10.1002/hyp.14787>